Research Article | Vol. 27, No. 13 | 24 Jun 2019 | OPTICS EXPRESS 18706
Optics EXPRESS

All optical control of comb-like coherent acoustic phonons in multiple quantum well structures through double-pump-pulse pump-probe experiments

C. Li,[1,*] V. Gusev,[2] T. Dekorsy,[1,3,5] and M. Hettich[1,4,6]

[1]Department of Physics and Center of Applied Photonics, University of Konstanz, Konstanz, D-78457, Germany
[2]Laboratoire d'Acoustique de l'Université du Mans (LAUM), UMR-CNRS 6613, Le Mans Université, Avenue O. Messiaen, 72085 Le Mans, France
[3]Department Institute for Technical Physics, German Aerospace Center (DLR), Stuttgart, D-70569, Germany
[4]Research Center for Non-Destructive Testing GmbH, 4040 Linz, Austria
[5]thomas.dekorsy@dlr.de
[6]mike.hettich@recendt.at
*changxiu.li@uni-konstanz.de

Abstract: We present an advancement in applications of ultrafast optics in picosecond laser ultrasonics - laser-induced comb-like coherent acoustic phonons are optically controlled in a $In_{0.27}Ga_{0.73}As$/GaAs multiple quantum well (MQW) structure by a high-speed asynchronous optical sampling (ASOPS) system based on two GHz Yb:KYW lasers. Two successive pulses from the same pump laser are used to excite the MQW structure. The second pump light pulse has a tunable time delay with respect to the first one and can be also tuned in intensity, which enables the amplitude and phase modulation of acoustic phonons. This yields rich temporal acoustic patterns with suppressed or enhanced amplitudes, various wave-packet shapes, varied wave-packet widths, reduced wave-packet periods and varied phase shifts of single-period oscillations within a wave-packet. In the frequency domain, the amplitude and phase shift of the individual comb component present a second-pump-delay-dependent cosine-wave-like and sawtooth-wave-like variation, respectively, with a modulation frequency equal to the comb component frequency itself. The variations of the individual component amplitude and phase shift by tuning the second pump intensity exhibit an amplitude valley and an abrupt phase jump at the ratio around 1:1 of the two pump pulse intensities for certain time delays. A simplified model, where both generation and detection functions are assumed as a cosine stress wave enveloped by Gaussian or rectangular shapes in an infinite periodic MQW structure, is developed in order to interpret acoustic manipulation in the MQW sample. The modelling agrees well with the experiment in a wide range of time delays and intensity ratios. Moreover, by applying a heuristic-analytical approach and nonlinear corrections, the improved calculations reach an excellent agreement with experimental results and thus enable to predict and synthesize coherent acoustic wave patterns in MQW structures.

© 2019 Optical Society of America under the terms of the OSA Open Access Publishing Agreement

1. Introduction

Owing to the rapid progress in the field of ultrafast lasers, the excitation and detection of short coherent acoustic phonons (CAPs) have become possible and have been intensively studied in various materials via ultrafast time-resolved spectroscopy [1–8]. Subsequently, CAP manipulation also has undergone active investigations, because of its underlying capabilities to upgrade our interests from monitoring to controlling phonon-relevant processes/devices, such as heat management in thermoelectric devices [9,10], phase-transition-memory devices [11,12], chemical potential modulation in crystals [13], effective

#362125 https://doi.org/10.1364/OE.27.018706
Journal © 2019 Received 12 Mar 2019; revised 28 May 2019; accepted 30 May 2019; published 19 Jun 2019

Optics EXPRESS

magnetic field stimulation in ferrite [14], integrated phononic circuitry [15], and acoustic nanocavities [16,17]. The straightforward way to manipulating CAPs on a picosecond time scale is to do so in tailored nanostructures and materials, since the properties of laser-induced coherent picosecond acoustic phonons are strongly dependent on the nature of the constituent layers, their thicknesses, and periods of layered structures or thin-films [18]. For example, frequencies and frequency differences within the observed triplets of zone-folded acoustic phonon modes were studied in GaAs/AlAs superlattices with different combinations of GaAs and AlAs monolayers [19]. In addition to the frequency, the acoustic amplitude and phase can also be modulated by the choice of layer thickness. In thin GaP films grown on a silicon substrate, both the amplitude and the phase of acoustic phonon time traces have been shown to vary with the GaP layer thickness in a wide range [20]. Material tailoring offers another possibility to adjust the acoustic phonon amplitude and frequency. For instance, $In_xGa_{1-x}N$ epilayers with various Indium composition x, led to a change of the amplitude of the acoustic oscillations proportional to the Indium composition [21]. Apart from the direct influence of sample structures and materials, the extrinsic factors such as external electric fields, temperature, pressure, and magnetic fields are also crucial to the CAP processes. Because the electronic properties of specific samples such as the energy band structure and dielectric constants can be tailored by temperature and pressure, additionally, the optical field inside materials can be modified by external electric and magnetic fields, leading to variations in light absorption and light scattering [22]. In turn, the photo-excited CAP processes are perturbed via electron-phonon, phonon-phonon and photon-phonon interactions. Hence, those extrinsic factors can also be applicable to tune acoustic phonons. For example, control of the CAPs amplitude was demonstrated by introducing external biases in a piezoelectric InGaN/GaN multiple quantum wells (MQWs) structure in the range from +2 V to –9 V [23]. The CAPs damping and amplitude were modulated by the temperature variation from 4.5 K to 300 K in a quantum cascade laser structure [24].

Even though the above approaches for CAP manipulation have displayed their feasibilities and versatilities, many questions remain open. While these questions could be answered by investigating a large number of different sample structures and using a large set of parameters for the variation of extrinsic factors, we decide to invest the control over CAP dynamics optically. Since CAPs are excited by lasers in ultrafast time-resolved spectroscopy, excited CAP features are considerably dependent on optical pulse properties. For example, the adjustment of pump light wavelength can result in the phonon pulse shape variation due to the altering of optical absorption spectra in a triple-quantum-well structure [25]. The optical pump power influence on the CAPs amplitude in a ZnO/ZnMgO MQWs structure, induced by the variation of photo-excited carriers and the screening effect, was also examined [26]. On the basis of the ultrafast optical single-pulse coherent control of CAP via optical pulse parameter modifications, the multiple-pulse optical manipulation of CAPs has arisen increasing attention and attained noticeable progress, which enables selective excitation in superlattices [27,28], MQW structures [29,30], nanoparticles [31], plasmonic nanostructures [32] and aluminum gratings [33], frequency tuneabilities in single quantum well structures [34] and thin films [35], and phase shifts in a MQW structure [36]. The multiple pulses are normally split from the pump source and adjustable time intervals between them are applied by introducing variable delay lines, hence constructive or destructive acoustic phonon excitations take place in the structure, depending on the time delay between them. More complex phonon control can be realized by simultaneous multi-parameter modulation of multiple optical pulses, which can take advantage of the ultrafast optical pulse shaping technique that enables user-defined almost arbitrary optical waveforms by a pulse shaper such as a spatial light modulator exerted on spectrally decomposed laser pulses [37]. Nonetheless, mere double-pump-pulse schemes have already proven their viability to manipulate CAPs by control of pump time intervals and pump intensities in semiconductor multilayer structures [28–30,36]. We notice several characteristics of the most reported two-pump-pulse optical

Optics EXPRESS

control systems of coherent acoustic phonons. Firstly, Nd-doped solid lasers pumped Ti:sapphire lasers are usually employed as pump and probe sources for pump-probe spectroscopy, which leads to high-cost and bulky systems. Secondly, the employed Ti:sapphire lasers mostly have a sub-GHz pulse repetition rate, which gives rise to a long time window (>1ns) that is not necessary for some CAP processes on the time scale of a few hundred ps. In addition, the systems with low repetition rate undergo a tradeoff between the scan rate and the temporal resolution [38]. Thirdly, most of the CAPs manipulation experiments are conducted in a conventional system where the time delay between the pump and the probe pulse is realized by a mechanical delay line, which limits the scan speed (<1 kHz) and thus the detection sensitivity that increases with the number of measurements accomplished in the fixed time interval. Last but not the least, in particular, to the best of our knowledge, the reported optically manipulated CAP oscillations [28–30,36] are not periodic wave-packet sequences. As an important step towards optically-dependent arbitrary acoustic waveform synthesis techniques via Fourier-transform spectral line-by-line shaping, the CAP wave-packet sequence deserves thorough investigations by means of double-pump-pulse optical manipulations. Zone-folded triplet modes have been previously excited in a GaAs/AlAs superlattice and were selectively enhanced or suppressed in a high-speed asynchronous optical sampling (ASOPS) system based on a pair of GHz Ti:sapphire lasers [28]. However, the acoustic oscillations were induced by unequally-spaced eigenmodes and thus non-periodic acoustic wave-packet waves. In addition, the systematic investigation of the simultaneous time delay and pump intensity control in the spectral domain was absent.

In this paper, we report on optical manipulation of CAPs by simultaneous tunable time delay and pump intensity of the second pump light pulse in a double-pump-pulse ASOPS system based on two GHz diode-pumped Yb:KYW lasers. The temporally periodic wave-packet-like and spectrally comb-like CAPs, are excited and optically manipulated in the periodic MQWs of a semiconductor saturable absorber mirror (SESAM). Resembling optical waveform synthesis, our result offers the possibility to dynamically shape the periodic acoustic wave-packet sequence by an all-optical method. The high detection sensitivity of our ASOPS system enables to follow already small changes in the controlled acoustic dynamics at a very low incident power of the second pump light. Previously we had reported only on CAPs excited in the same sample in a single-pump-pulse configuration [39,40], which only presented elementary interpretations of CAPs generation, propagation and detection in the MQWs and established a basic understanding of the relevant dynamics. In order to elucidate the acoustic modulation taking place in the double-pump-pulse process, we develop a simplified theoretical model, which is initially applied to the analysis of the single-pump-pulse system, and is subsequently advanced to cope with the more complicated double-pump-pulse situation, and is finally optimized by two approaches. Our to-be-shown research results demonstrate how ultrafast optics continues to advance one of its application fields – laser ultrasonics. Specifically, our results show the promising ability of a GHz-Yb:KYW-laser ASOPS system to optically manipulate complex acoustic phonons. To the best of our knowledge, such a system has been applied to investigate the multi-pulse optical coherent control of CAPs by ultrafast time-resolved spectroscopy for the first time, which potentially stirs new applications and continuing progress in laser ultrasonics.

2. Experimental set-up and sample

Double-pump-pulse experiments are performed in the ASOPS system based on two Yb:KYW lasers, as shown in the block diagram in Fig. 1(a). The two lasers are working at a pulse repetition rate level of 1 GHz, with a small repetition rate difference of 5 kHz stabilized by a phase-locked loop (f_{pump} = 1 GHz + 5 kHz, f_{probe} = 1 GHz), emitting at a central wavelength of ~1050 nm. The detailed set-up description can be found in our previous report [39]. The system performance is characterized in terms of temporal resolution and detection sensitivity. The temporal resolution is about 500 ps after considering the increment (~100 ps) over 1-ns

Optics EXPRESS

time window due to the relative timing jitter between the two lasers. The temporal resolution is limited by the laser pulse duration (the pump and probe laser pulse durations are ~210 ps and ~280 ps, respectively).The detection sensitivity is close to shot noise limit (noise floor can be below $\Delta R/R = 10^{-6}$ in a few seconds). Differing from the original single-pump-pulse set-up, the incident pump beam is split into two portions by a pellicle before collinearly irradiating the sample in the normal direction. In the path of one of the split beams, a variable mechanical delay stage is inserted in order to control the time interval between two pump pulses, as illustrated in Figs. 1(b) and 1(c). For the adjustment of the pump intensity of the delayed pump pulse, an adjustable neutral density filter (NDF) and a half wave plate (HWP) are employed and inserted in the path of the delayed pulse. The NDF is capable of tuning the pump power in the range of 0 – 37 mW and the HWP can extend the tunable range from 37 mW to 69 mW due to the pellicle transmission dependences on polarizations. The probe beam is oblique with respect to the sample and its power is fixed at 4.5 mW. The reflectivity variation of the sample after its excitation by the pump laser pulse is a function of the time delay between the probe pulse and pump pulses, which is monitored by the reflected probe light.

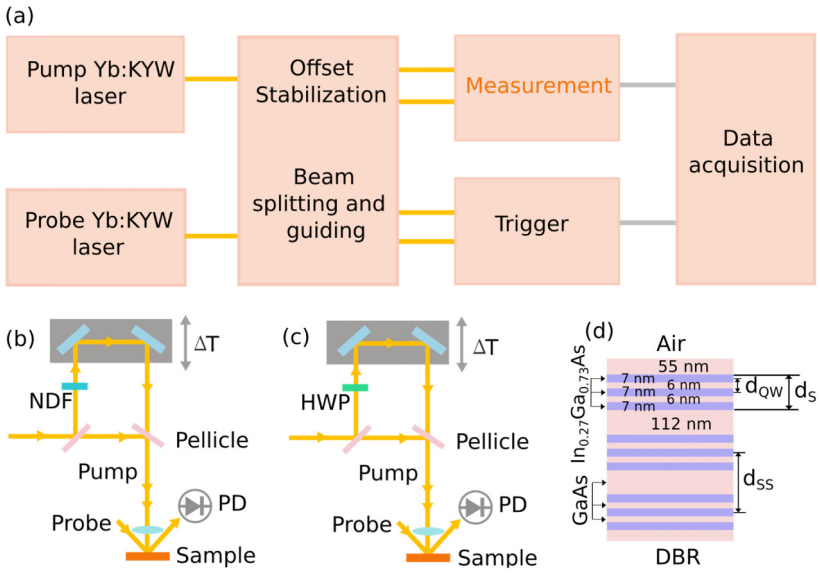

Fig. 1. (a) The block diagram of ASOPS system. (b) The double-pump-pulse configuration in the measurement box. NDF: neutral density filter. NDF is used to adjust the delayed second pump power in the range of 0 – 37 mW. (c) The supplementary double-pulse-pump configuration in the measurement box. HWP: half wave plate. HWP is used to adjust the delayed second pump power in the range of 37 – 69 mW. (d) The sample structure. The multilayered sample is composed of GaAs layers (coral pink areas), $In_{0.27}Ga_{0.73}As$ layers (QW, blue areas) and a DBR.

The sample under investigation is a SESAM structure with multiple $In_{0.27}Ga_{0.73}As$ quantum wells (QWs) as saturable absorber ahead of a distributed Bragg reflector (DBR) consisting of 23 pairs of $GaAs/Al_{0.95}Ga_{0.05}As$. The DBR reflects the incident light with a reflectance of nearly 100%. Because the photon energy is above the bandgap of $In_{0.27}Ga_{0.73}As$ but below the bandgap of DBR constituent materials in the structure, light absorption occurs only in the QWs. The structure of the sample is displayed in Fig. 1(d). The sample is grown on a GaAs substrate along the [100] direction. Every three QWs and their barriers form a triple-QW stack and in total three triple-QW stacks are formed. All QWs have the same thickness of 7 nm and all barriers within a triple-QW stack also have the same thickness of 6 nm. The GaAs layer thickness between two adjacent triple-QW stacks is 112 nm while the

Optics EXPRESS

thickness of the GaAs cap layer is 55 nm, which is approximately half of the stack-to-stack distance. To clarify the notations, d_{QW} denotes the distance between two adjacent QWs, which also indicates the wavelength of laser-induced acoustic phonons in QWs; d_s denotes the thickness of the triple-QW stack; d_{ss} denotes the stack-to-stack distance. It will take excited longitudinal acoustic phonons a time duration of $T = d_{ss}/v \approx 30.2$ ps to travel through adjacent triple-QW stacks (v = 4730 m/s in GaAs [41]). Because the periodic MQW structure is of great interest for wave-packet-like coherent acoustic phonon manipulations, our following acoustic discussions will focus on this region rather than the DBR. All experiments are performed at room temperature.

3. Theoretical modelling

Once a pump photon is absorbed inside the QW region, electron-hole pairs are excited. Hence, the electronic distribution in the QWs is disturbed and thus an initial stress is set up in each QW via deformation potential [42]. The detailed stress distribution largely depends on the space-time evolution of photo-excited charge carriers and physical properties of the structure [2]. However, a detailed microscopic treatment of the electron dynamics is beyond the scope of this work. As we will show in the following this does not hinder an already in depth understanding of the undergoing acoustic dynamics.

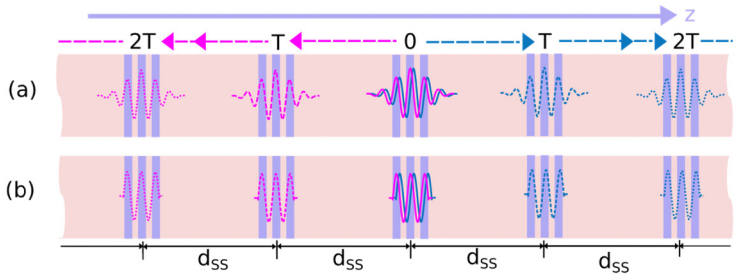

Fig. 2. Illustration of the stress wave initiated in a triple-QW stack (solid curves) and detected periodically (dotted lines) in an infinite MQW structure. The profile of a triple-QW stack is assumed as (a) Gaussian shape and (b) rectangular shape.

Based on the structure of the triple-QW stack where the thickness of InGaAs is very close to that of the GaAs barrier $d_{InGaAs} \approx d_{barrier}$, and the wave-packet-like acoustic oscillations displayed in our earlier measurements [39,40], it is reasonable to assume that the stress wave generated in each triple-QW stack is a cosine wave enveloped by the profile of the stack. For simplicity, we will initially assume that the stack generation profile exhibits a Gaussian shape. The launched stress wave propagates simultaneously forward and backward along the z-axis which is perpendicular to the QWs (see Fig. 2(a)). Due to the small acoustic impedance difference between $In_{0.27}Ga_{0.73}As$ and GaAs, the acoustic reflections on the interfaces are neglected in our following analysis. In addition, considering that the counter-propagating stress waves have the equivalent impact on the final acoustic response, we will not specify the stress wave propagation direction in our mathematical analysis. To begin with, we consider the excitation by a single pump pulse in one triple-QW stack. The generated stress wave can be expressed as a function of space z and time t

$$f_g(z,t) = a\exp\left[-\frac{(z-vt)^2}{2\sigma^2}\right]\cos\left[\frac{2\pi}{d_{QW}}(z-vt)\right], \quad (1)$$

where a is a constant, indicating the stress wave amplitude, v denotes the longitudinal acoustic velocity in the sample, d_{QW} denotes the QW-to-QW distance. Because the sound velocities are nearly equal $v_{InGaAs} \approx v_{GaAs}$ [40], for simplicity in the modelling, we assume that acoustic

Optics EXPRESS

waves are travelling everywhere in the MQW structure at the speed of $v = v_{GaAs}$. The standard deviation σ in the Gaussian formula can be given as

$$\sigma = \frac{d_s}{2\sqrt{2\ln 2}}, \tag{2}$$

where d_s denotes the triple-QW stack thickness, defined as the full width at half maximum (FWHM) of the Gaussian profile. When the stress waves travel along the z-axis in the sample, the vibration perturbs the refractive index and thus the probe light will monitor its modifications via photoelastic effect. In our ASOPS system, the probe Yb:KYW laser is nearly identical to the pump laser in terms of the central wavelength, the pulse-width, and the pulse repetition rate. Thereby, the stress detection sensitivity function is assumed to share the same form with the stress generation function, written as a function of z

$$f_d(z) = \mathrm{b}\exp\left(-\frac{z^2}{2\sigma^2}\right)\cos\left(\frac{2\pi}{d_{QW}}z\right), \tag{3}$$

where b is a constant. Equation (3) only represents the detection sensitivity function of a single triple-QW stack, for the compact presentation of the following integration calculation. The final acoustic waves detected by all triple-QW stacks will be discussed later where necessary. The induced temporal signal response can be regarded as the convolution of the stress wave generation function and the detection sensitivity function

$$s_1(t) = f_d(z) * f_g(z) = \int_{-\infty}^{\infty} f_d(z) f_g(z,t)\,\mathrm{d}z. \tag{4}$$

If Eqs. (1) and (3) are substituted into Eq. (4), the following expression is obtained:

$$\begin{aligned} s_1(t) &= \int_{-\infty}^{\infty} \mathrm{ab}\exp\left[-\frac{z^2}{2\sigma^2}-\frac{(z-vt)^2}{2\sigma^2}\right]\cos\left[\frac{2\pi}{d_{QW}}(z-vt)\right]\cos\left(\frac{2\pi}{d_{QW}}z\right)\mathrm{d}z \\ &= \frac{1}{2}\mathrm{ab}\exp\left[-\left(\frac{vt}{2\sigma}\right)^2\right]\left[\mathrm{c}_1+\mathrm{c}_2\cos\left(\frac{2\pi}{d_{QW}}vt\right)\right] \\ &\cong \mathrm{c}_3\exp\left[-\left(\frac{vt}{2\sigma}\right)^2\right]\cos\left(\frac{2\pi}{d_{QW}}vt\right). \end{aligned} \tag{5}$$

In Eq. (5), c_1, c_2 and c_3 are constants. The integral calculation indicates $\mathrm{c}_1 \cong 0 \ll \mathrm{c}_2$, therefore, c_1 can be ignored. The final expression in Eq. (5) is associated with the high-frequency oscillation which shows a wave-packet-like behavior. Then we will perform Fourier transform to $s_1(t)$ as follows

$$\begin{aligned} S_1(f) &= \int_{-\infty}^{\infty} s_1(t)\exp(-i2\pi ft)\,\mathrm{d}t \\ &= \mathrm{c}_4\left(\exp\left\{-\left[\frac{f-f_0}{v/(2\pi\sigma)}\right]^2\right\}+\exp\left\{-\left[\frac{f+f_0}{v/(2\pi\sigma)}\right]^2\right\}\right), \end{aligned} \tag{6}$$

where c_4 is a constant and $f_0 = v/d_{QW}$, indicating the frequency of acoustic oscillation in the triple-QW stack. The result in Eq. (6) implies that the envelope of the acoustic spectrum also has a Gaussian shape with the central frequency f_0 and the bandwidth $\Delta B_{FWHM} = (\ln 2)^{1/2} v/(\pi\sigma)$. It is noteworthy that the spectrum is real, which means the spectral phase equals zero in the frame of our modelling. So far only a single triple-QW stack is taken into account

Optics EXPRESS

in the acoustic phonon generation and detection process. However, the triple-QW stack spatially repeats with the equal distance d_{ss} in the structure, which means the stress waves initiated in the triple-QW stack subsequently propagate in both forward and backward directions, and are detected in the equally distributed triple-QW stacks at times $t = nd_{ss}/v = nT$, where n = 1, 2, 3, … (see Fig. 2(a)). As the illustration indicates, the MQW structure is assumed to be infinite along the z- axis, which permits us not to take into consideration the reflection on the air/sample boundary and simplifies the calculation. Because the cap layer thickness approximately equals half of the thickness of the GaAs layer sandwiched by two neighboring triple-QW stacks, the assumption of simply repeated triple-QW stacks without the air/sample interface reflection makes sense in our calculation. In addition, it is worthwhile mentioning that the stress waves are excited in all triple-QW stacks at the same time although only the excitation by a single triple-QW stack is illustrated and analyzed above. The combined excitation by all the triple-QW stacks only leads to larger acoustic intensity compared to a single triple-QW stack excitation. Finally, concerning the damping of the wave-packet sequence potentially induced by defect scattering, the stress wave sign change by the reflection on the air/GaAs interface, and the limited number of triple-QW stacks in the physical structure, we assume that the time-domain acoustic signal is enveloped by a Gaussian shape $h(t)$. Hence, taking into account the temporally periodically repeated wave-packets, the overall damping and the amplitude magnification, the final acoustic response can be expressed as

$$\begin{aligned} s_{1\_\mathrm{total}}(t) &= \mathrm{c}_5 \sum_{n=-\infty}^{\infty} s_1\left(t-\frac{nd_{ss}}{v}\right) h(t) \\ &= \mathrm{c}_5 \sum_{n=-\infty}^{\infty} s_1\left(t-\frac{nd_{ss}}{v}\right) \exp\left[-\frac{1}{2}\left(\frac{2\sqrt{2\ln 2}}{\Delta t}\right)^2 t^2\right], \end{aligned} \tag{7}$$

where c_5 is a constant and Δt represents the pulsewidth (FWHM) of the superimposed Gaussian envelope. The Fourier transform is then applied to Eq. (7) as follows

$$\begin{aligned} S_{1\_\mathrm{total}}(f) &= \int_{-\infty}^{\infty} \mathrm{c}_5 \sum_{n=-\infty}^{\infty} s_1\left(t-\frac{nd_{ss}}{v}\right) h(t) \exp(-i2\pi f t)\,\mathrm{d}t \\ &= \mathrm{c}_6 \sum_{m=-\infty}^{\infty} S_1(f) H(f-m\Delta f), \end{aligned} \tag{8}$$

where c_6 is a constant, m is an integer, and Δf denotes the spectral comb spacing with the relation $\Delta f = v/d_{ss}$. $H(f)$ represents the Fourier transform of $h(t)$. We then substitute Eq. (6) into Eq. (8) and apply a Fourier transformation to $h(t)$, so the final acoustic spectrum in the MQW structure analyzed in the single-pump-pulse configuration can be presented as

$$\begin{aligned} &S_{1\_\mathrm{total}}(f) = \\ &\mathrm{c}_7 \sum_{m=-\infty}^{\infty} \left(\exp\left\{-\left[\frac{f-f_0}{v/(2\pi\sigma)}\right]^2\right\} + \exp\left\{-\left[\frac{f+f_0}{v/(2\pi\sigma)}\right]^2\right\} \right) \exp\left\{-\left[\frac{f-m\Delta f}{2\sqrt{2\ln 2}/(\pi\Delta t)}\right]^2\right\}, \end{aligned} \tag{9}$$

where c_7 is a constant. Equation (9) reveals four features of the spectral response. Firstly, the amplitude spectrum is composed of comb-like components spaced by Δf which is determined by the triple-QW stack-to-stack spacing and the longitudinal acoustic velocity. The spectrum is real. Secondly, the comb spectrum is centered at f_0, determined by QW-to-QW spacing within a triple-QW stack and the longitudinal acoustic velocity. Thirdly, the comb components amplitude is enveloped by a Gaussian shape associated with the acoustic generation and detection profile in the triple-QW stack. Equation (9) together with Eq. (2), indicates that the bandwidth of the comb spectrum is inversely proportional to the thickness

Optics EXPRESS

of the triple-QW stack. Lastly, the comb linewidth is related to the acoustic temporal damping window duration.

In the same way, if a rectangular generation and detection profile with width equal to d_s in the triple-QW stack is assumed (see Fig. 2(b)), the following spectrum can be derived

$$S_{1R\_total}(f) = c_8 \sum_{m=-\infty}^{\infty} \left(\frac{1}{(f-f_0)^2} \left\{ \sin^2 \left[\frac{f-f_0}{v/(\pi d_s)} \right] \right\} + \frac{1}{(f+f_0)^2} \left\{ \sin^2 \left[\frac{f+f_0}{v/(\pi d_s)} \right] \right\} \right) \exp \left\{ - \left[\frac{f-m\Delta f}{2\sqrt{2\ln 2}/(\pi \Delta t)} \right]^2 \right\}, \quad (10)$$

where c_8 is a constant. Unlike the spectrum under the assumption of a Gaussian profile, the spectrum derived from a rectangular generation and detection profile, shows that the acoustic comb components are modulated by the square of a sampling function and thus show a clear distinction regarding spectral bandwidth and comb component amplitudes compared to the Gaussian assumption.

We will now move on to the double-pump-pulse situation, performing the analysis in the spectral domain. Two key variables are introduced to demonstrate the acoustic manipulation by a double-pump-pulse scheme, namely, the time delay ΔT between the first and the second pump pulse and the pump power ratio $q = P_2/P_1$ where P_1 and P_2 are the pump power for the first and the second beam, respectively. For a given pump laser, the pump pulse intensity is proportional to the pump power and slight beam spot size variations induced by divergence when ΔT is adjusted are ignored, so the pump power ratio is considered the same as pump pulse intensity ratio in our analysis. We start with a brief discussion of the pump power effect. As a saturable absorber incorporated in the SESAM structure, the $In_{0.27}Ga_{0.73}As$ QW layers lead to a nonlinear reflectivity curve dependent on the incident pulse fluence, because the saturation absorption takes place when the initial states for the pump light transitions are bleached while the final states are still occupied at high optical pump fluence [43,44]. Therefore, the amplitude of photo-excited acoustic phonons potentially does not follow a linear relation with the incident pump power as well. However, initially we will assume that the phonon amplitude is proportional to the incident pump power for simplicity as follows

$$\frac{A_2}{A_1} = \frac{P_2}{P_1} = q, \quad (11)$$

where A_2 and A_1 denote the amplitude of CAPs excited by the first pump pulse and by the second pump pulse, respectively. In Section 4, we will improve our model by nonlinear corrections. Secondly, in addition to the varied pump power, the excitation by the sequential pump light with changing time intervals ΔT also gives rise to subtle modifications of carrier dynamics in the QWs [45], which is interesting for preventing multi-pulsing phenomena or for the development of high repetition rate lasers by observing the optical absorption. However, we will not further explore its effect on acoustic phonons, but simply neglect the potential consequence in the modelling. In the time domain, the double-pump-pulse induced acoustic response can be written as

$$s_{2\_total}(t) = s_{1\_total}(t) + q s_{1\_total}(t - \Delta T). \quad (12)$$

The corresponding acoustic response in the spectral domain is thus derived as follows

$$\begin{aligned} S_{2\_total}(f) &= S_{1\_total}(f) + q S_{1\_total}(f) \exp(-i2\pi f \Delta T) \\ &= \left| S_{2\_total}(f) \right| \exp\left[i\theta(f) \right]. \end{aligned} \quad (13)$$

The amplitude spectrum $|S_{2\_total}(f)|$ and phase spectrum $\theta(f)$ can be expressed as

Optics EXPRESS

$$\left|S_{2\_\text{total}}(f)\right| = \left|S_{1\_\text{total}}(f)\right| \sqrt{(1-q)^2 + 4q\cos^2(\pi f \Delta T)} \tag{14}$$

and

$$\theta(f) = \tan^{-1}\left[\frac{-q\sin(2\pi f \Delta T)}{1+q\cos(2\pi f \Delta T)}\right], \tag{15}$$

respectively. Equations (14) and (15) indicate that both the acoustic spectral amplitude and phase are modulated simultaneously by the pump intensity ratio q and the time delay between two successive pump pulses ΔT. Several interesting facts are unveiled as follows. Firstly, when q is fixed, the amplitude variation of the spectral comb components is periodic with varying ΔT. Moreover, the frequency of the periodic variation is equivalent to the spectral frequency f. Secondly, if the comb frequency $f = m\Delta f$ (m = 1, 2, 3, …) is substituted into Eq. (14), the local minimum of the spectral amplitude variation with q can be found at q = 1 for the mth comb component where m satisfies $m = (2n + 1)/(2\Delta f \Delta T)$ (n = 0, 1, 2, …) and is an integer number for the particular values of ΔT. Thirdly, the spectral phase also shows a periodic variation dependent on ΔT, when q is fixed.

In the next section, the experimental CAP results attained in the double-pump-pulse ASOPS system will be given, meanwhile, the modelling will be visualized for comparison.

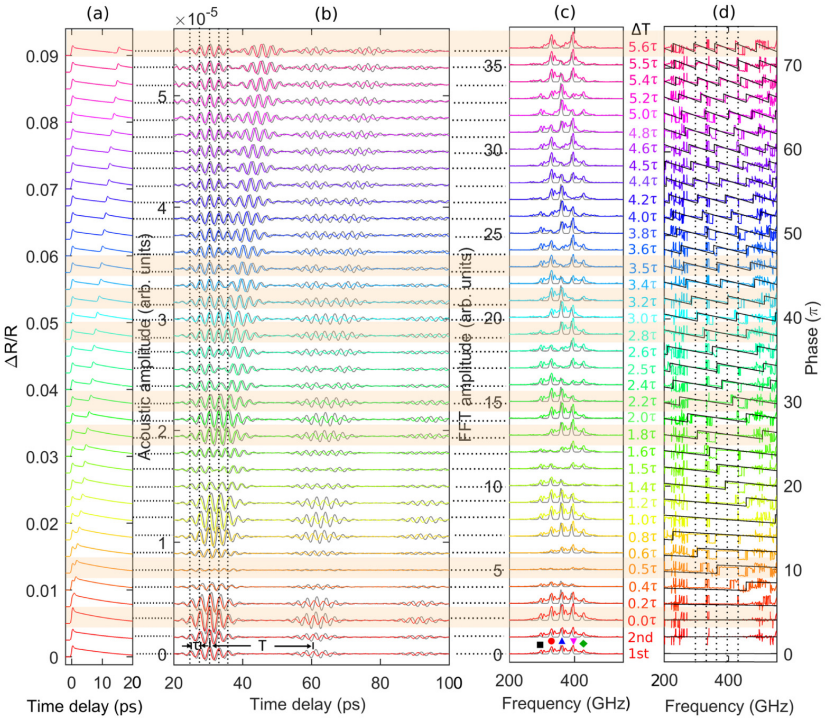

Fig. 3. (a) Original time traces, (b) coherent acoustic phonons, (c) acoustic amplitude spectrums, and (d) acoustic phase spectrums when the second pump time delay ΔT varies in the range of 0 – 5.6τ (0.5T). The first pump power P_1 equals the second pump power P_2 of 27 mW. Curves with ΔT-dependent color represent experimental results and gray curves represent modelling results given Gaussian generation and detection functions in individual triple-QW stack. Vertical dot black lines in (d) indicate the positions of five comb frequencies. Data are shifted vertically for clarity in steps of 2.5×10^{-3} in (a), 1.5×10^{-6} in (b), 1 in (c) and 2π in (d).

Optics EXPRESS

4. Experimental results and modelling visualization

For clarification, experimental acoustic waves presented in this section are obtained by numerically removing the electronic and thermal exponential decaying background from the original reflectivity change (ΔR/R) traces via a smoothing average method. Thus the small acoustic signal becomes visible and coherent control over acoustic waves can be observed.

4.1 Tunable pump delay, fixed pump power

Previously we have described and discussed CAPs excited in the same MQW structure by a single-pump-pulse ASOPS system based on two Yb:KYW lasers, where an acoustic wave-packet temporal sequence was produced, due to spatially periodically distributed triple-QW stacks [39,40]. Aiming to optically coherently controlling the CAPs in this structure, a second pump pulse with tunable time delay ΔT and tunable pump power P_2 is introduced in the experimental set-up.

Initially, the optical power of the second pump light is kept equal to that of the first one at 27 mW, meanwhile, the time delay ΔT between two pump pulses is adjustable in the range from 0 to $0.5T$ (5.6τ) which equals 15.12 ps in our case by moving a variable delay stage, where T and τ denote the period of the acoustic wave-packet sequence and the period of oscillations within the individual acoustic wave-packet, respectively. Consequently, a series of distinct coherent acoustic phonons is obtained by tuning only the time delay ΔT and displayed by curves with ΔT-dependent color in Figs. 3(a)-3(d) in forms of the original pump-probe time traces, the subtracted temporal acoustic phonons, and the acoustic spectral amplitudes and spectral phases. For comparison, the single-pump-pulse measurements with only the first pump beam and only the second pump beam incident are performed, as depicted in the first and second curves at the bottom of Figs. 3(a)-3(d). The five equally spaced pronounced frequency comb components at f_1 = 297.8 GHz, f_2 = 330.5 GHz, f_3 = 363.2 GHz, f_4 = 396.4 GHz and f_5 = 428.2 GHz are defined as comb1, comb2, comb3, comb4 and comb5 (from left to right, marked by a black, red, blue, magenta and green symbol in Fig. 3(c)), respectively, which will be discussed in terms of acoustic amplitude and phase variations throughout Section 4. Compared to the single-pump-pulse acoustic phonons, the double-pump-pulse acoustic phonons amplitudes are evidently enhanced at $\Delta T = 0.0\tau$ and suppressed at $\Delta T = 0.5\tau$ for all five comb components. Subsequently, they are also enhanced at $\Delta T = 1.0\tau$, 2.0τ, 3.0τ, 4.0τ while almost cancelled out at $\Delta T = 1.5\tau$, 2.5τ, 3.5τ, 4.5τ in the temporally overlapping region of the wave-packets excited by the first pump pulse and those excited by the second pump pulse. Depending on the time delay ΔT, it is possible to almost extinguish certain frequency comb components. For instance, at $\Delta T = 1.8\tau$, 2.2τ, 2.8τ, 3.2τ, and 3.5τ, comb1, comb5, comb2, comb4, and comb3 are greatly suppressed, respectively. In other words, all five comb components can be individually controlled to be present or absent in the spectrum by selecting a specific time delay ΔT, which could be very useful for filtering out the unwanted acoustic spectral components if required in certain applications. At the specific time delay $\Delta T = 5.6\tau \cong 0.5T$, it is noticeable that odd spectral components are suppressed, leading to a doubled frequency comb spacing and a reduced temporal wave-packet period to $T/2$.

Not only the spectral amplitude but also the spectral phase is dependent on the second pump time delay ΔT, as shown in Fig. 3(d). In order to eliminate the initial phase caused by the temporal range selection (20 – 250 ps) for Fourier transform and other potential perturbations in the experiment, the spectral phase resulting from the double-pump-pulse set-up is displayed as a result of relative spectral phase with respect to that obtained in the single-pump-pulse set-up. The simultaneous spectral amplitude and phase modulation by tuning ΔT, enables a variety of acoustic wave-packet sequences, where the shape, the width and the amplitude of the individual wave-packet can be modified flexibly, leading to a quasi-arbitrary acoustic wave-packet shaping, as depicted in Fig. 3(b). The maxima corresponding to single-

Optics EXPRESS

period oscillations composing an individual wave-packet experience phase shifts approximately from - π to π, depending on ΔT. For example, the oscillation at 35.6 ps is out of phase at $\Delta T = 1.4\tau$ compared to the single-pump-pulse data (the fifth peak in the first wave-packet in Fig. 3(b)). Based on the theoretical modelling in the last section, the acoustic calculation under the assumption of a Gaussian triple-QW generation and detection profile is applied in the condition of tunable ΔT and fixed $q = 1$, as depicted by solid gray (black) curves in Figs. 3(b)-3(d). The comparison of experimental curves and calculation curves indicates that our modelling achieves good agreement with the experimental results in the tunable ΔT range in both the temporal and spectral domain.

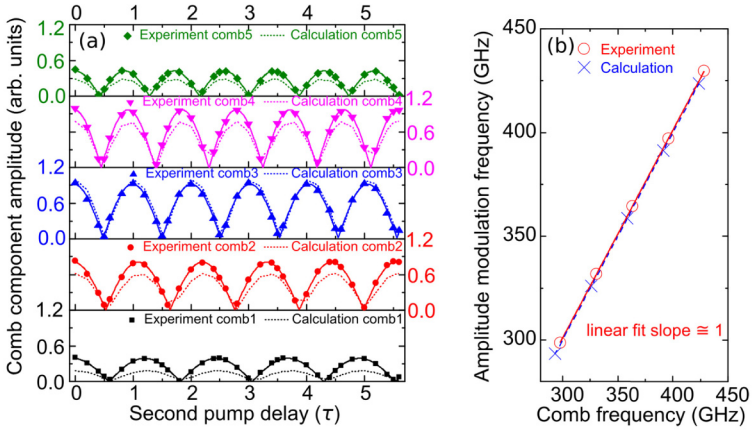

Fig. 4. (a) The amplitude of five main frequency comb components at 297.8 GHz, 330.5 GHz, 363.2 GHz), 396.4 GHz and 428.2 GHz as a function of the second pump time-delay from 0 to 5.6τ. Solid lines denote the absolute cosine fit for experimental results by $y(t) = |\cos(\pi f t)|$. (b) The relation between the modulation frequencies from (a) and the corresponding comb component frequencies.

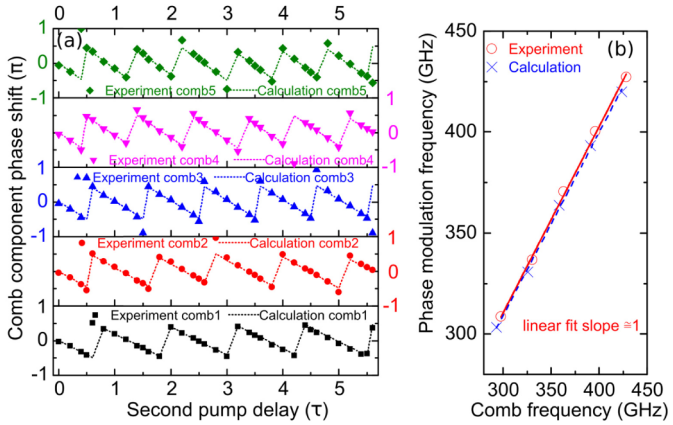

Fig. 5. (a) The phase shift of five main frequency comb components at 297.8 GHz, 330.5 GHz, 363.2 GHz, 396.4 GHz and 428.2 GHz as a function of the second pump delay from 0 to 5.6τ. (b) The relation between the phase modulation frequencies from (a) and the corresponding comb component frequencies.

The slight discrepancy between the experiment and the modelling (~0.3 ps for peaks in the first wave-packet and ~5 GHz for spectral comb components) can be attributed to the uncertainty of determination of the acoustic velocity in the sample and the nominal QW-to-QW width and stack-to-stack width. The high baseline shown in experimental amplitude spectrum is mainly caused by numerical Fourier transform window. Because the strongest

Optics EXPRESS

wave-packets are at the beginning of the time delay and the wave-packet sequence has a fast decay, a sharp-edged window is used to preserve the main signal so that the spectral information will be more reliable although a high baseline can be caused. The baseline can be lower if a Gaussian-like window is chosen, however, most visible wave-packets would be suppressed in this case, leading to a weak noisy spectrum. Potentially, the high baseline could be partly caused by the sample fabrication issues such as inhomogeneities and defects. The unexpected spectral phase jump and the irregular phase appearing in the experiment could be caused by the experimental noise (the acoustic signal is small beyond the range approximately from 290 GHz to 430 GHz, so the phase in those small-signal regimes is easy to be disturbed by the noise) and numerical operations. The lateral phase deviation between experiments and calculations probably stems from the imperfect accuracy to determine ΔT by adjusting the variable translation stage.

In order to find out how the spectral comb amplitude and phase are quantitatively dependent on the second pump delay ΔT, the amplitude and phase of the five main spectral comb components are extracted from Figs. 3(c) and 3(d). In Fig. 4(a), ΔT-dependent amplitudes of comb1, comb2, comb3, comb4 and comb5, display an apparent cosine-wave-like variation, with a peak amplitude ratio of 0.40:0.83:0.94:1.00:0.43 and a decreasing period of $\tau_1 = 1.23\tau$, $\tau_2 = 1.11\tau$, $\tau_3 = 1.01\tau$, $\tau_4 = 0.93\tau$ and $\tau_5 = 0.86\tau$, respectively. On the one hand, the periodic evolution of individual comb components at different speed permits various comb amplitude profiles and the periodic removal of a certain component. On the other hand, a complete extinction of all comb components at the same ΔT is not possible. At $\Delta T = 0.5\tau$, only comb3 is almost completely suppressed and other four comb components remain finite although with a small amplitude. The cosine-wave-like behavior can be explained very well by Eq. (14) in Section 3, where the spectral amplitude is modulated by a factor $|\cos(\pi f \Delta T)|$ when $q = 1$, indicating that the amplitude evolution with the time delay ΔT is a periodic variation following modulus of cosine with a frequency of f. Importantly, the factor reveals that the modulation frequency of this variation for a comb component is exactly equivalent to the frequency of the comb component itself. We illustrate the relation of the frequency of the five amplitude modulations from Fig. 4(a) and the corresponding frequency of comb components in Fig. 4(b) where the linear fit slope is very close to 1, which clearly corroborates our above interpretations. Like the spectral amplitude evolution, the spectral phase also exhibits a periodic variation, depending on the second pump delay ΔT (see Fig. 5(a)). However, the phase shift curve for each comb component is sawtooth-wave-like in the phase range approximately from $-\pi/2$ to $\pi/2$. The linear fit with a slope of $\cong 1$ in Fig. 5(b) also indicates that the frequency of phase modulation equals the frequency of the corresponding comb component. The explanation of the periodic behavior can be found in Eq. (15), where the inverse tangent contains a numerator of $-\sin(2\pi f \Delta T)$ and a denominator of $1 + \cos(2\pi f \Delta T)$ (when $q = 1$) which are both periodic waves with a frequency of f as a function of ΔT, leading to the periodic phase shift evolution with the period of $1/f$ for the comb component with a frequency of f. At last, by illustrating simultaneous spectral amplitude modulation (see Fig. 6(a)) and phase modulation (see Fig. 6(b)) in the range of the second pump delay $\Delta T = 0 - 5.6\tau$ with tiny ΔT steps, we emphasize several points in the following.

Firstly, both the spectral amplitude and the spectral phase dependences on ΔT change faster when the spectral frequency is higher, leading to numerous amplitude and phase combinations for the main five comb components.

Secondly, our result offers another approach to measure the frequency of acoustic phonons, considering that the frequency of the periodic spectral amplitude and phase dependences on ΔT for a comb component equals the frequency of the comb component itself.

Thirdly, the amplitude of each comb component is restricted in the range from 0 to $2|S_{1\_total}(f)|$, where $|S_{1\_total}(f)|$ represents the spectral component amplitude of single-pump-pulse acoustic phonons, while the spectral phase is restricted in the range from $-\pi/2$ to $\pi/2$. The $\pi/2$

Optics EXPRESS

(or -π/2) phase restriction is attributed to the fact that the denominator 1 + cos(2πfΔT) periodically equals zero when ΔT satisfies ΔT = (2n + 1)/ (2f) (n is an integer).

Fourthly, the produced temporal acoustic wave-packet sequences as a consequence of simultaneous spectral amplitude and phase modulation demonstrate various interference patterns of acoustic phonons, which shape the discrete individual wave-packets, depending on the second pump delay ΔT, as shown in Fig. 6(c).

To sum up, by only adjusting the time delay ΔT between two successive optical pump pulses in the range of 0 – 5.6τ, we have experimentally shown that acoustic phonons are coherently controlled by periodic comb amplitude and comb phase modulations, leading to an almost complete suppression of certain comb components at certain time delays ΔT, which is well supported by our theoretical modelling.

In addition to the second pump delay ΔT, the pump power ratio q is also adjustable in our system. Hence, in the following we will explore whether it is feasible to modulate acoustic phonons by tuning q at a fixed ΔT. For example, we will examine if the almost extinct comb component can be revived by changing q and if the spectral amplitude and phase range can be extended compared to the case where q = 1.

4.2 Tunable pump power, fixed pump delay

4.2.1 Pump delay ΔT = 0.5τ

As the first example, we introduce the adjustment of the pump ratio q at the fixed ΔT = 0.5τ which gives rise to immense acoustic suppression at q = 1. In the experiment, the power of the first pump light is fixed at 27 mW while that of the second pump light is tunable from 3 mW to 67 mW. The experimental and theoretical results are present in Figs. 7(a)-7(d). The experimental results (see curves with q-dependent color) will be discussed first.

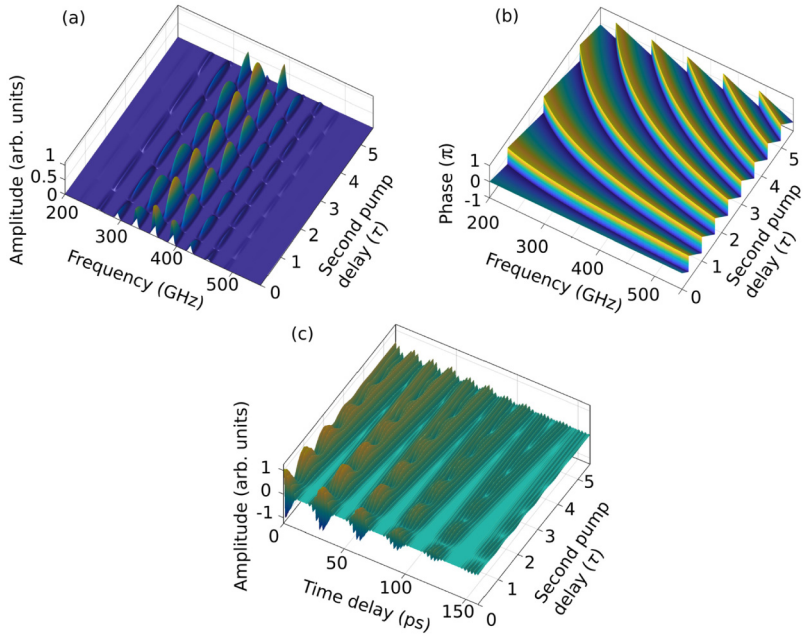

Fig. 6. The acoustic calculation based on the assumption of a Gaussian generation and detection profile of the triple-QW stack. The pump power ratio is fixed at q = 1 and the second pump pulse delay ΔT is adjustable in the range of 0 – 5.6τ . (a) The comb frequency component amplitude dependences on the second pump pulse delay. (b) The comb frequency component phase dependences on the second pump pulse delay. (c) The corresponding variation of coherent acoustic phonons as a function of the second pump pulse delay.

Optics EXPRESS

Although the acoustics are greatly suppressed at q = 27/27, the spectral comb components are not completely wiped out by adjusting the second pump delay ΔT. As indicated in Fig. 7(c), the complete removal can be realized by fine tuning q in the vicinity of q = 1 neither, which can be interpreted with the assistance of Eq. (14) where the amplitude modulation factor $[(1 - q)^2 + 4q\cos^2(\pi f\Delta T)]^{1/2}$ exhibits zero value at $\Delta T = 0.5\tau$ only in the condition of q = 1 and $f = (2m + 1)/\tau$ (m is an integer). Due to the relation $1/\tau \approx f_3$, the factor has a dip only at comb3 while the other four comb components can be suppressed to some extent because they are in the vicinity of the dip. On the contrary, tuning q enables the suppressed comb components to grow gradually back when $q > 1$ and $q < 1$ (see Fig. 7(c)). Take comb3 for instance, the amplitude ratio at q = 3/27, 27/27, 67/27 is 0.92:0.08:0.88 obtained from the experimental results, which proves that acoustic phonons can also be modulated by tuning the pump power ratio q. It is worth noticing that the comb amplitude has a minimum at around q = 27/27 and displays a saturation feature at high q (see Fig. 7(c)), and the comb phase also shows a saturation tendency when q > 27/27 (see Fig. 7(d)). The phase variation with frequency is slow, which is caused by the large period $2/\tau \cong 2f_3$ at $\Delta T = 0.5\tau$ based on Eq. (15).

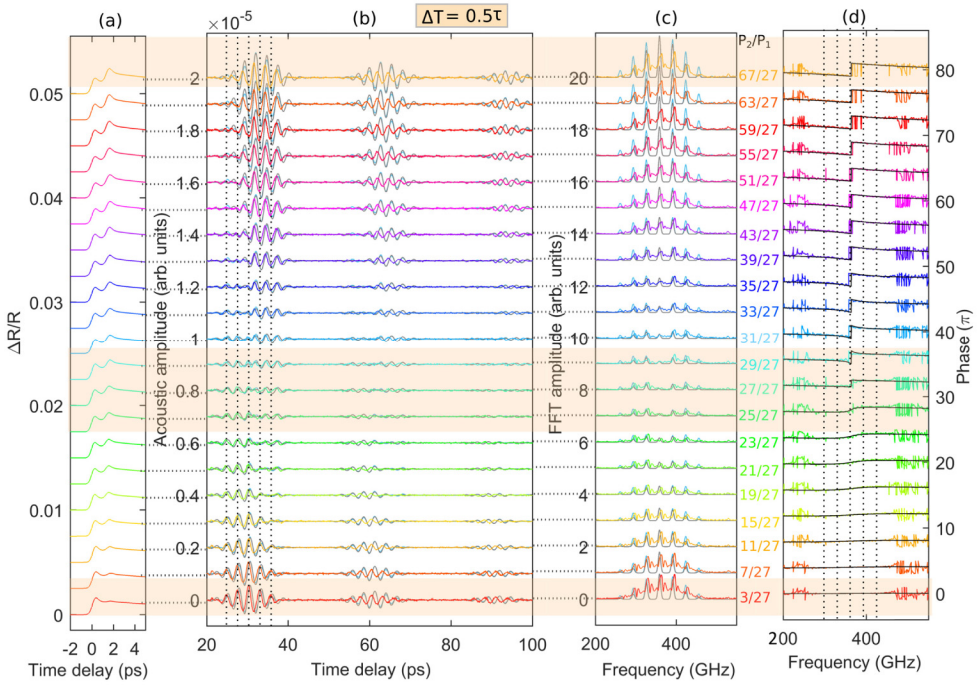

Fig. 7. Comparison of experimental, Gaussian and rectangular modelling results. The pump power ratio $q = P_2/P_1$ varies from 3/27 to 67/27 and the second pump delay is fixed at 0.5τ. The first pump power is fixed at 27 mW in experiments. (a) Original time traces. (b) Coherent acoustic phonons. (c) Acoustic amplitude spectrums. (d) Acoustic phase spectrums. Curves with q-dependent color represent experimental results. Gray curves in (b) and (c) represent Gaussian modelling results. Sky blue curves in (b) and (c) represent rectangular modelling results. Black solid curves in (d) represent modelling results. Vertical dot black lines in (d) indicate the position of five comb components. Data are shifted vertically for clarity in steps of 2.5×10^{-3} in (a), 1.0×10^{-6} in (b), 1 in (c) and 4π in (d).

In the temporal domain, acoustic phonons also experience interesting alterations (see Fig. 7(b)). Firstly, the leading part or the trailing part of the individual wave-packet can be selectively suppressed. For example, at around q = 21/27, the trailing half part is suppressed, while at around q = 35/27, the leading half part is suppressed. Secondly, some single-period

Optics EXPRESS

oscillations composing the wave-packet undergo a phase shift of π when q is approximately larger than 27/27 with respect to those at q = 3/27. At q = 67/27, all oscillations inside the wave-packet exhibit a phase shift of π, which means the whole wave-packet sequence is delayed by 0.5τ with respect to that at q = 3/27 (see the top curve and the bottom curve in Fig. 7(b)). For comparison, the acoustic calculations under the assumption of a Gaussian and rectangular triple-QW profile are both given in the case of tunable q and fixed $\Delta T = 0.5\tau$, which are illustrated in Figs. 7(b) and 7(c) by gray curves and sky-blue curves, respectively. The phase calculation is illustrated by black curves in Fig. 7(d). As can be seen, the temporal acoustic waves and the spectral amplitude and phase in general fit well with the experimental results.

However, at high q, the calculation of the temporal acoustic amplitude and the spectral amplitude obviously surpasses the corresponding experimental amplitude, because a linear relation between pump power and acoustic amplitude is assumed in the calculation. Hence, in the following a nonlinear factor k_0 for spectral comb components, which should make pump-power-acoustic-amplitude relation more realistic, will be introduced to improve our modelling.

Moreover, the assumption of a Gaussian triple-QW detection and generation profile yields a spectral bandwidth of 89.5 GHz, which is smaller than the experimental bandwidth of 109.6 GHz, leading to a comparatively smaller amplitude for comb1 and comb5 in the single-pump-pulse experiment. The assumption of a rectangular one produces a spectral bandwidth of 127.6 GHz in the single-pump-pulse experiment, which is larger than the experimental bandwidth, leading to additional dominant comb components. In addition, the overall normalized component-to-component amplitude ratios show a discrepancy between the calculation and the experiment (experiment: 0.4:0.86:0.96:1:0.5, Gaussian: 0.2:0.6:1:0.8:0.3, rectangular: 0.4:0.8:1:0.9:0.5). Although a rectangular stress envelope is theoretically expected, the finite detection and generation bandwidth can smear out the rectangular shape, which potentially accounts for the deviation between the modelling and experiment results regarding the spectral bandwidth and envelope. Because the double-pump-pulse modelling is based on the single-pump-pulse analysis, the effect from the imperfect generation and detection function is also impinged upon the double-pump-pulse acoustic phonons, as illustrated in Figs. 7(b) and 7(c) at low q. Hence, we will also improve the spectral envelope in the following by a heuristic-analytical method.

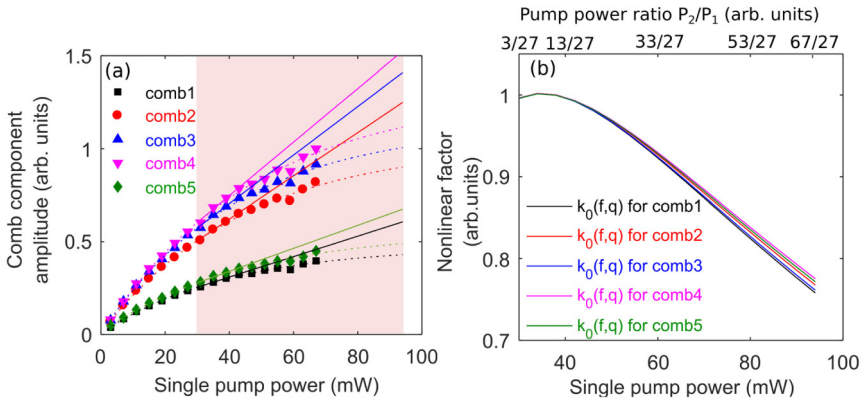

Fig. 8. (a) The experimental comb component amplitude dependences on the pump power when only the second pump beam is incident on sample (filled symbols). The pump power varies from 3 mW to 67 mW. The amplitude curves of five comb components are individually fit linearly from 30 mW and exponentially from the beginning. Solid lines represent the linear fit and dot lines represent the nonlinear fit. The nonlinear factor k_0 (f, q) is the ratio between the nonlinear fit and the linear fit. (b) Nonlinear factor curves $k_0(f, q)$ for five comb components in the range of pump power ratio $q = P_2/P_1$ from 3/27 to 67/27.

Optics EXPRESS

In order to determine the value of the nonlinear factor k_0, experiments with only the second pump incident on the sample are performed in the range of the pump power from 3 to 67 mW with steps of 4 mW. As shown in Fig. 8(a) (filled symbols in five colors), the acoustic spectral amplitude has a nonlinear relation with the incident pump power, which intrinsically stems from the saturation absorption in the QWs of our sample and thus a nonlinear reflectivity curve. An exponential fit is applied to the experimental data for five comb components, starting from the lowest pump power (see dot lines in Fig. 8(a)), meanwhile, a linear fit is applied to the experimental data starting from 30 mW (see solid lines in Fig. 8(a)). The nonlinear factor k_0 is a result of ratio between the exponential fit and the linear fit ranging from 30 mW to 94 mW of the single pump power, as depicted in Fig. 8(b). Such a fitting range is selected, because in the two-pulse-pump experiments the total incidence $P_1 + P_2$ ranges from (27 + 3) mW to (27 + 67) mW. The nonlinear factor k_0 can be thus expressed as a function of f and q

$$k_0(f,q) = \frac{A_1(f)\exp\left[27(1+q)/t_1(f)\right] + A_0(f)}{a_0(f) + 27b_0(f)(1+q)}, \tag{16}$$

where $A_1(f)$, $t_1(f)$ and $A_0(f)$ are exponential fitting parameters at $f = f_1, f_2, f_3, f_4, f_5$, while $a_0(f)$ and $b_0(f)$ are linear fitting parameters at $f = f_1, f_2, f_3, f_4, f_5$. The nonlinear factor is then multiplied with the amplitude spectrum Eq. (14) to correct the exceeded acoustic amplitude at high pump power induced by a linear relation assumption.

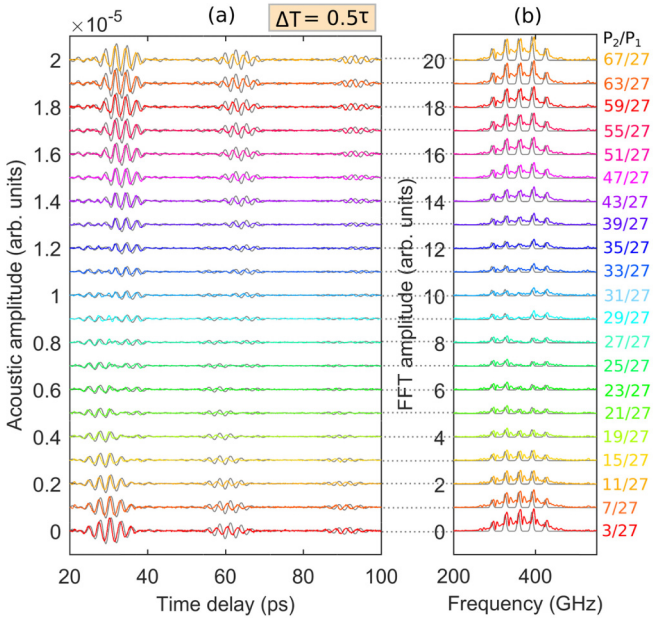

Fig. 9. Comparison of experimental and heuristic-analytical results after nonlinear corrections in the range of q from 3/27 to 67/27 at $\Delta T = 0.5\tau$. (a) Time domain coherent acoustic phonons and (b) corresponding acoustic spectrum series. Curves with q-dependent color represent experimental results and gray lines represent the results after nonlinear corrections. Data are shifted vertically for clarity in steps of 1.0×10^{-6} in (a) and 1 in (b).

The improvement of the generation and detection function is indirectly achieved by using the experimental single-pump-pulse comb amplitude $|S_{1\_exp}(f)|$ featured by the comb components ratio 0.4:0.86:0.96:1:0.5 at 27 mW instead of using the derived $|S_{1\_total}(f)|$ or $|S_{1R\_total}(f)|$ in Eq. (14). By combination of the nonlinear factor k_0 corrections and heuristic-analytical envelope corrections, the improved results are produced and displayed in Figs. 9(a)

Optics EXPRESS

and 9(b) (gray curves). In consequence, the acoustic phonons obtained from the improved modelling fit well with the experimental acoustic phonons in the entire q range in both the temporal and spectral domain. In Fig. 10(a), the amplitude of individual comb components dependences on q after improvement by above two approaches (open symbols) in general achieves a better agreement with experimental amplitude (filled symbols) than Gaussian-based calculations after nonlinear factor corrections (dot lines) and rectangular-based calculation after nonlinear factor corrections (cross signs). A few data points obtained from the heuristic-analytical method show slightly larger deviations from experimental data at low q than those obtained from the rectangular modelling do, however, this will not affect the general improvements. The improved spectral amplitude is restricted by $k_0(f, q)|S_{1\_exp}(f)|[(1 - q)^2 + 4q\cos^2(\pi f\tau/2)]^{1/2}$. Because the cosine term is close to zero at $\Delta T = 0.5\tau$ for all five comb components, the determination factor of the spectral amplitude can be regarded as $k_0(f, q)|S_{1\_exp}(f)(1 - q)|$, which is smaller than $2|S_{1\_exp}(f)|$ for all considered q.

In Fig. 10(b), the comb phase shift dependences on q demonstrate that, firstly, the phase shift for all spectral comb components ranges approximately from 0 to π (or – π to 0); secondly, the phase shift sign of comb1 and comb2 is opposite to that of comb4 and comb5; thirdly, comb3 exhibits an abrupt phase change from ~0 to - π at around q = 1 (a few experimental data points are discarded for comb3 due to their unexpected jump to the positive side. This perhaps stems from the incorrect sign determination in the numerical phase extraction. This also could be attributed to the inaccuracy of ΔT adjustment, which causes phase shifts from the desired value and thus a sudden jump when the phase is close to the wrapped phase "cliff" π (-π) (see Fig. 7(d)).); lastly, the phase saturation at high q can be understood with the help of Eq. (15) where the right side term can be also written as $\tan^{-1}\{-\sin(2\pi f\Delta T)/[1/q + \cos(2\pi f\Delta T)]\}$. Because $1/q$ approaches zero when q is large enough, the term can be approximated as $\tan^{-1}[-\tan(\pi)]$ at $\Delta T = 0.5\tau \cong 0.5f_3$ for comb3, implying -π phase at high q. Due to $fi/f_3 \approx 1$ (i = 1, 2, 4, 5), the phase for four other comb components is close to π (or -π) at high q.

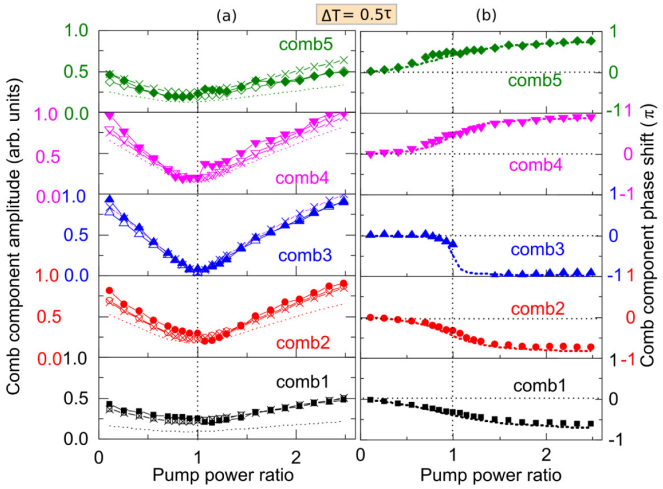

Fig. 10. (a) The comb component amplitude dependences on the pump power ratio $q = P_2/P_1$ at $\Delta T = 0.5\tau$. Filled symbols connected by solid lines represent experimental results. Open symbols connected by solid lines represent heuristic-analytical results after nonlinear corrections. Cross symbols connected by solid lines represent rectangular modelling results after nonlinear corrections. Dot lines represent Gaussian modelling results after nonlinear corrections. (b) The comb component phase dependences on the pump power ratio $q = P_2/P_1$ at $\Delta T = 0.5\tau$. Filled symbols represent experimental data and dot curves represent calculation data. Gray straight lines are only for marking purpose.

Optics EXPRESS

4.2.2 Pump delay $\Delta T = 2.8\tau$, 3.0τ, 3.2τ

In addition to $\Delta T = 0.5\tau$, we also perform acoustic phonon manipulation by tuning the pump power ratio at $\Delta T = 2.8\tau$, 3.0τ, 3.2τ for demonstration. When $q = 1$, the factor $|\cos(\pi f \Delta T)|$ modulates the spectral amplitudes (see Fig. 4(a)). Then the following statements can be concluded: at $\Delta T = 2.8\tau$, comb2 can be greatly suppressed because of the dip of comb2 at $2.5\tau_2 = 2.78\tau$; at $\Delta T = 3.0\tau$, comb1 and comb5 can be both greatly suppressed because of one dip of comb1 at $2.5\tau_1 = 3.08\tau$ and one dip of comb5 at $3.5\tau_5 = 3.01\tau$; at $\Delta T = 3.2\tau$, comb4 can be greatly suppressed because of one dip of comb4 at $3.5\tau_4 = 3.26\tau$. τ_i (i = 1, 2, 3, 4, 5) is the period of the cosine-wave-like amplitude dependences on ΔT for the comb component with the frequency f_i (i = 1, 2, 3, 4, 5), which were already defined in Section 4.1.

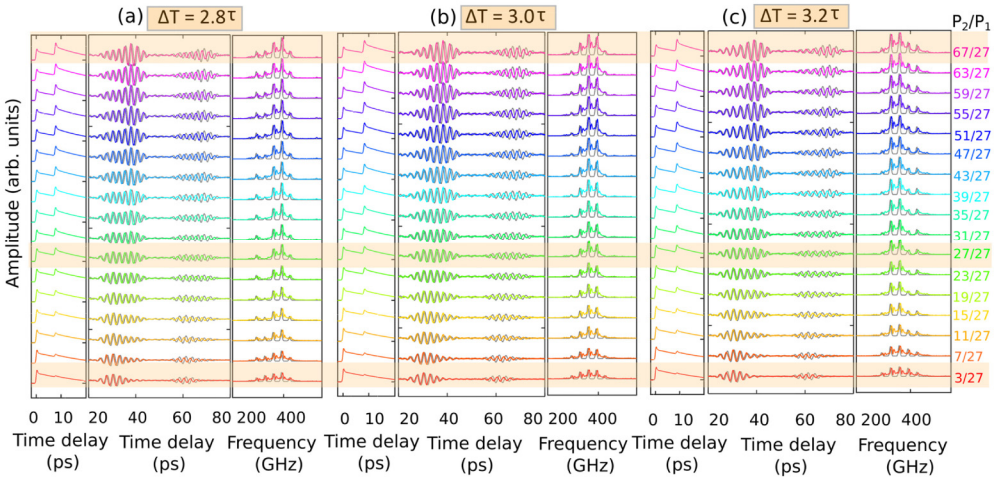

Fig. 11. The original time traces (left), coherent acoustic phonons (middle) and FFT spectrum series (right) when the second and the first pump power ratio varies from 3/27 to 67/27. (a) ΔT is fixed at 2.8τ. (b) ΔT is fixed at 3.0τ. (c) ΔT is fixed at 3.2τ. Curves with q-dependent color represent experimental results and gray curves represent heuristic-analytical results after nonlinear corrections. Data are shifted vertically for clarity.

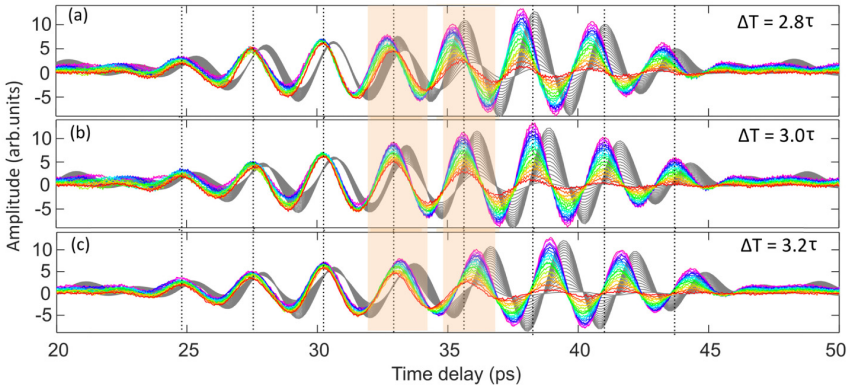

Fig. 12. The first wave-packet of acoustic phonons when the pump power ratio varies from 3/27 to 67/27 (the data are the same as those in Figs. 11(a)-11(c), but smaller steps are used for the vertical shift). The second pump delay is (a) $\Delta T = 2.8\tau$, (b) $\Delta T = 3.0\tau$, (c) $\Delta T = 3.2\tau$. Vertical dot gray lines indicate the peak positions in the case of $\Delta T = 3.0\tau$ at the pump ratio q = 3/27 (red). The colored curves from red to magenta represent experimental data from q = 3/27 to 67/27 (same as those curves in Figs. 11 (a)-11(c)). The gray curves represent heuristic-analytical results after nonlinear corrections.

Optics EXPRESS

As illustrated in Figs. 11(a)-11(c), when ΔT keeps fixed, all the previously suppressed comb components can be gradually revived by decreasing q or increasing q from q = 1, meanwhile, other comb components in general experience a monotonically increasing variation when q is increased from the lowest to the highest value. It is worth mentioning that even at the lowest q = 3/27 (the second pump power is only 3 mW) the modulation made by introducing the second pump is still totally visible. At the lowest q, the normalized component-to-component amplitude ratios at $\Delta T = 2.8\tau$, 3.0τ, 3.2τ are 0.38:0.63:0.85:1:0.41, 0.34:0.75:1:0.95:0.35, 0.36:0.89:1:0.8:0.38, respectively. The capability to reveal an acoustic manipulation at a very low pump power can be attributed to the high detection sensitivity of our ASOPS system.

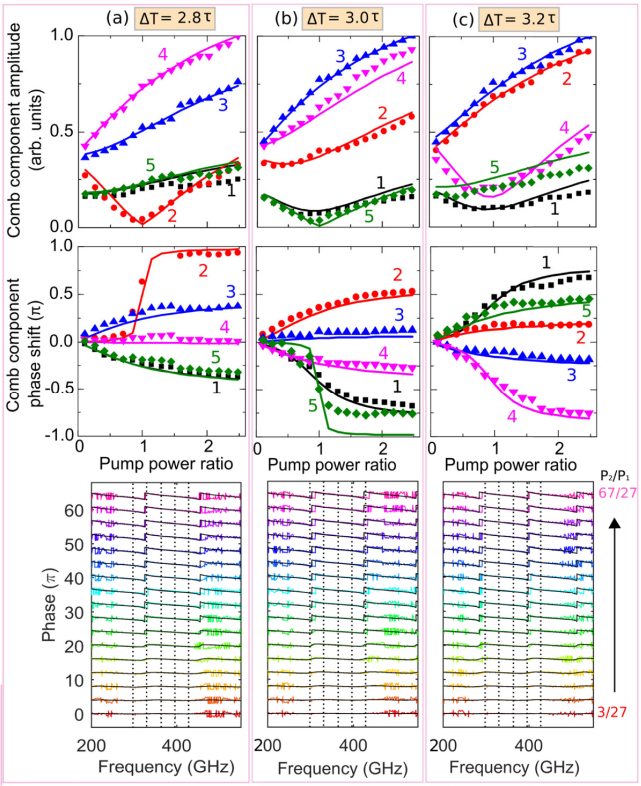

Fig. 13. Frequency comb component amplitude and phase dependences on the pump power ratio q. (a) The second pump delay is fixed at 2.8τ. Top: comb component amplitude dependences on q. Middle: comb component phase shift dependences on q. Filled symbols denote experimental data, while solid lines denote heuristic-analytical results. The numbers 1, 2, 3, 4, 5 are used to address five comb components defined in Section 4.1. Bottom: spectral phase in the q range from 3/27 to 67/27 in steps of 4/27. Curves with q-dependent color represent experimental results and solid black curves represent heuristic-analytical results after nonlinear corrections. Vertical dot black lines indicate the position of five comb components. Phase spectrums are vertically shifted for clarity in steps of 4π. (b) The second pump delay is fixed at 3.0τ. (c) The second pump delay is fixed at 3.2τ.

In the time domain, acoustic sequences composed of wave-packets with a variety of profiles are produced. Because the wave-packet generated by the first pump and that generated by the second pump light are nearly half-overlapped and have a constructive interference at around $\Delta T = 3.0\tau$, the wave-packet remains a Gaussian-like shape whose width is effectively prolonged, showing up to 8 single-period oscillations within each wave-packets. Apart from the amplitude, the rise time of the wave-packet profile leading edge and the fall time of the wave-packet trailing edge can be tuned by q. The comparison of the improved

Optics EXPRESS

modelling based results (gray curves in Figs. 11(a)-11(c)) with experimental results (curves with q-dependent color in Figs. 11(a)-11(c)) demonstrates an excellent agreement in the tunable q range at $\Delta T = 2.8\tau$, 3.0τ, 3.2τ in both the temporal and spectral domain. In order to find out the subtle temporal pulse phase shift caused by tuning q, acoustic sequences are shifted vertically in smaller steps (see Figs. 12(a)-12(c)). It is noticeable that the fourth oscillation at 32.9 ps and the fifth oscillation at 35.65 ps have a positive phase shift (maximum 0.15π (4th) and 0.26π (5th)) at $\Delta T = 2.8\tau$, a negative phase shift (maximum -0.11π (4th) and -0.26π (5th)) at $\Delta T = 3.2\tau$, while a zero phase shift at $\Delta T = 3.0\tau$, by tuning q. At $\Delta T = 2.8\tau$ and 3.2τ, the maximum phase shift of single-period oscillations cannot reach π by tuning q, while that can be achieved at $\Delta T = 0.5\tau$ by tuning q.

The spectral amplitude and phase dependences on the pump power ratio q for the five main spectral comb components at $\Delta T = 2.8\tau$, 3.0τ, 3.2τ are displayed in Figs. 13(a)-13(c). In terms of the spectral amplitude dependences on q, the following points can be summarized.

Firstly, the amplitude dependences on q for some comb components are non-monotonic while those for some other comb components monotonically increase with q. The selection of comb component with a quadratic-function-like shape whose valley is at $q = 1$, depends on the factor $[(1 - q)^2 + 4q\cos^2(\pi f\Delta T)]^{1/2}$ which indicates that the zero minimum only exists at $q = 1$ and $f = (2m + 1)/(2\Delta T)$ (m is an integer). Therefore, at $\Delta T = 2.8\tau \cong 2.8/f_3$ and $m = 2$, the zero minimum can be found approximately at $f = 5f_3/5.6 \approx f_2$ (see the top of Fig. 13(a)); at $\Delta T = 3.0\tau \cong 3.0/f_3$ and $m = 2, 3$, the zero minimum can be found approximately at $f = 5f_3/6 \approx f_1$ and $f = 7f_3/6 \approx f_5$ (see the top of Fig. 13(b)); at $\Delta T = 3.2\tau \cong 3.2/f_3$ and $m = 3$, the zero minimum can be found approximately at $f = 7f_3/6.4 \approx f_4$ (see the top of Fig. 13(c)). In order to explain the local minimum point in the range of $0 \le q \le 1$, we have to rely on the general local minimum expression of $q = -\cos(2\pi f\Delta T)$, which indicates that the minimum exists in the range $0 \le q \le 1$ when $f\Delta T$ satisfies $(4n + 1)/4 \le f\Delta T \le (4n + 3)/4$ (n is an integer). For example, the comb1 amplitude at $\Delta T = 3.2\tau$ has a minimum at $q = 0.73$ (see the top of Fig. 13(c)). When the minimum is located in the range $-1 \le q \le 0$ under the condition $(4n + 3)/4 \le f\Delta T \le (4n + 5)/4$ or $0 \le f\Delta T \le 1/4$ (n is an integer), we will observe a monotonically increasing amplitude behavior of some spectral comb components. For example, the comb3 amplitude dependence on q has a consistently rising tendency at $\Delta T = 2.8\tau$, due to the fact that the minimum of the quadratic function locates at $q = -0.31$ (see the top of Fig. 13(a)).

Secondly, the maximum amplitude is restricted by the expression $k_0(f, q)|S_{1\_exp}(f)|[(1 - q)^2 + 4q\cos^2(\pi f\Delta T)]^{1/2} \le 2.6|S_{1\_exp}(f)|$, which means that in Figs. 13(a)-13(c), unlike the case in Section 4.1 and the case at $\Delta T = 0.5\tau$, the comb component amplitude can exceed $2|S_{1\_exp}(f)|$ at high q and proper $f\Delta T$. For example, the maximum of comb3 amplitude at $\Delta T = 3.0\tau$ is larger than $2|S_{1\_exp}(f_3)| \approx 2A_3(q = 3/27)$ ($A_3(q)$ denotes the amplitude of comb3, see the top of Fig. 13(b)).

In terms of the spectral phase dependences on q, the following points can be summarized.

Firstly, at $\Delta T = 2.8\tau$, 3.0τ, 3.2τ, the phase shift of all comb components shows a saturation effect at high q, which can be explained in the similar way to the case at $\Delta T = 0.5\tau$.

Secondly, only a certain comb component can reach π or $-\pi$ phase shift, which is determined by whether the condition $2f\Delta T \approx 2n + 1$ (n is an integer) in $\tan^{-1}[-\tan(2\pi f\Delta T)]$ is satisfied. For example, comb2 at $\Delta T = 2.8\tau$ can reach π due to $2 \times 2.8f_2\tau \approx 5$ (see the middle of Fig. 13(a)); comb5 at $\Delta T = 3.0\tau$ can reach approximately $-\pi$ due to $2 \times 3.0f_5\tau \approx 7$ (see the middle of Fig. 13(b)); comb4 at $\Delta T = 3.2\tau$ can reach up to approximately $-\pi$ due to $2 \times 3.2f_4\tau \approx 7$ (see the middle of Fig. 13(c)). However, the abrupt phase change around $q = 1$ takes place only when the relation of f and ΔT satisfies $2f\Delta T = 2n + 1$ (n is an integer) perfectly.

Thirdly, the modelling agrees also well with the experiment in the whole tunable q range at $\Delta T = 2.8\tau$, 3.0τ, 3.2τ in terms of spectral phase (see figures in the second line and the third line of Figs. 13(a)-13(c)). The phase variations with the varying frequency at $\Delta T = 2.8\tau$, 3.0τ,

Optics EXPRESS

3.2τ are faster than that at $\Delta T = 0.5\tau$, because the corresponding variation periods $f_3/2.8$, $f_3/3.0$ and $f_3/3.2$ along frequency axis based on Eq. (15) are smaller.

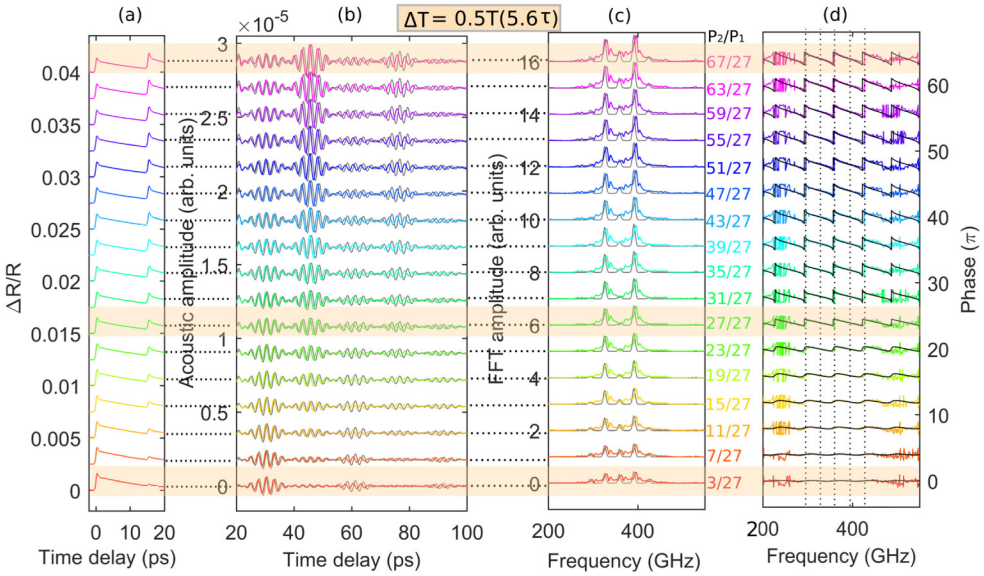

Fig. 14. (a) Original time traces, (b) coherent acoustic phonons, (c) acoustic amplitude spectrum and (d) acoustic phase spectrum when the second pump delay is fixed at 5.6τ (0.5T) and the pump power ratio varies from 3/27 to 67/27. The first pump power is fixed at 27 mW in experiments. Curves with q-dependent color represent experimental results. Gray (black) curves represent heuristic-analytical results after nonlinear corrections. Vertical dot lines in (d) indicate the position of five comb components. Data are vertically shifted for clarity in steps of 2.5×10^{-3} in (a), 1.8×10^{-6} in (b), 1 in (c), and 4π in (d).

4.2.3 Pump delay $\Delta T = 0.5T$

At last, the acoustic phonon manipulation by tuning q at $\Delta T = 0.5T$ (5.6τ) is demonstrated, as illustrated in Figs. 14(a)-14(d). Because the second pump delay is half of the wave-packet period, the acoustic wave-packets generated by the first pump light temporally are well separated with those generated by the second pump light (see Fig. 14(b)), which enables not only the wave-packet sequence period reduction from T to $T/2$ but also the modulation of the amplitude ratio of adjacent wave-packets. The amplitude ratio between the first wave-packet (centered at 30.25 ps) and the second wave-packet (centered at 45.4 ps) ranges from 1:0.27 to 1:2.07 by tuning q from 3/27 to 67/27. In the spectral domain, the simultaneous extreme suppression of comb1, comb3 and comb5 is achieved at q = 1. This can be understood from Fig. 4(a) where $A_1(4.5\tau_1) \cong A_3(5.5\tau_3) \cong A_5(6.5\tau_5) \cong 0$ ($A_i(\Delta T)$ denote the amplitude of the comb component comb$i$ (i = 1, 3, 5) at the second pump pulse delay ΔT) can be satisfied at the same second pump delay ΔT = 5.6τ. The suppression of all odd comb components can also be interpreted from the perspective of the frequency modulations revealed by us theoretically in Section 3. The spectral modulation factor $|\cos(\pi f T/2)|$ can be written as $|\cos[\pi m\Delta f/(2\Delta f)]|$ because the wave-packet period ΔT is the inverse of comb spacing Δf and the acoustic comb frequency is determined by $f = m\Delta f$ (m is an integer), which means that only the odd frequency comb components can be suppressed ($m = 2n + 1$, n is an integer) when the factor equals zero. If we count from the beginning of frequency axis, comb1, comb3 and com5 are the 9th, the 11th and the 13th frequency components ($f_1/\Delta f \cong 9, f_3/\Delta f \cong 11, f_5/\Delta f \cong 13$). Like the cases where ΔT = 0.5τ, 2.8τ, 3.0τ, 3.2τ, at ΔT = 0.5T, the suppressed comb components can also be gradually revived by either decreasing q or increasing q from q = 1. However, as can be observed (see Fig. 14(c)), the normalized component-to-component amplitude ratio cannot

Optics EXPRESS

be totally recovered even at the lowest q or the highest q, differing from the $\Delta T = 0.5\tau$ case where the normalized component-to-component amplitude ratios at low q and high q are very close to that of acoustic phonons generated by the single-pump-pulse set-up. The spectral phase is periodic along the frequency axis. The period remains the same at $2\Delta f$ regardless of the variation of q, while the maximum phase is adjustable from 0 to π by tuning q (see Fig. 14(d)). Compared to all periodic acoustic phase dependences on frequency that we have discussed so far (ΔT = 0.5τ, 2.8τ, 3.0τ, 3.2τ), the one at $\Delta T = 0.5T$ exhibits the fastest variations. As proved in Figs. 14(b)-14(d), the modelling results (gray curves) agree well with the experimental results (curves with q-dependent color) at $\Delta T = 0.5T$.

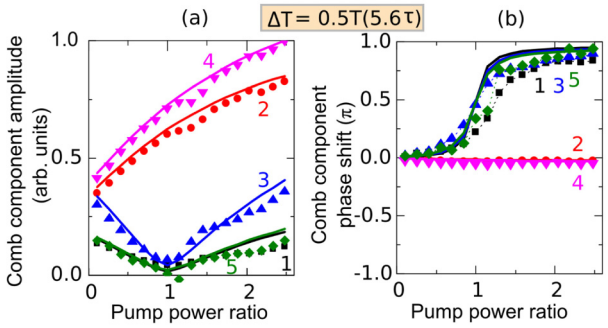

Fig. 15. (a) Comb component amplitude and (b) comb component phase shift dependences on pump power ratio q, when the second pump delay is fixed at 5.6τ ($0.5T$). Filled symbols denote experimental data, while solid lines denote heuristic-analytical results. The numbers 1, 2, 3, 4, 5 are used to address five comb components defined in Section 4.1.

As for individual spectral line modulations, the amplitudes of comb1, comb3, and comb5 dependences on q are of non-monotonic shape, while those of comb2 and comb4 are monotonic with increased q (see Fig. 15(a)). Because $f_i/\Delta f$ (i = 2, 4) is an even number, the upper amplitude levels of comb2 and comb4 are approximately restricted at $2.6|S_{1\_exp}(f)|$ based on the expression $k_0(f, q)|S_{1\_exp}(f)|[(1 - q)^2 + 4q\cos^2(\pi f/(2\Delta f))]^{1/2}$ at q = 67/27, while the amplitudes of comb1, comb3, and comb5 are limited approximately below $1.1|S_{1\_exp}(f)|$ due to the fact that the cosine term falls to zero when $f_i/\Delta f$ (i = 1, 3, 5) is an odd number. The above statement is an explanation of why the suppressed comb components cannot be totally recovered by tuning q (see Fig. 14(c)). The q-dependent spectral phase shift of individual comb components shown in Fig. 15(b) reveals that, interestingly, all odd comb components experience the similar phase variation which displays a leap at around q = 1 as well as a tendency of approaching to π at high q, while all even comb components undergo the similar variation which displays an almost constant zero phase shift. The explanation can be found in Fig. 14(d), where phase-frequency relation exhibits a constant $2\Delta f$ period, leading to odd comb components at peak of the sawtooth-like curve and even comb components at the middle of slope (zero phase). It also makes sense to interpret the phase curves by use of Eq. (15), where the numerator $-q\sin(2\pi f/(2\Delta f))$ equals zero at f_i (i = 2, 4) due to the fact that $f_i/\Delta f$ (i = 2, 4) is an even number, leading to a zero phase for even comb components in the whole tunable q range, while the denominator $1 + q\cos(2\pi f/(2\Delta f))$ equals zero at q = 1 and f_i (i = 1, 3, 5) due to the fact that $f_i/\Delta f$ (i = 1, 3, 5) is an odd number, leading to a phase of π/2. When q is high enough, the phase for comb components at f_i (i = 1, 3, 5) is approaching $\tan^{-1}[-\tan(2\pi f/(2\Delta f_i))]$ (i = 1, 3, 5) which is approximately wrapped to π.

To sum up, the CAP manipulation by tuning the pump power ratio q at a fixed second pump delay ΔT = 0.5τ, 2.8τ, 3.0τ, 3.2τ, $0.5T$ (5.6τ) has been discussed. The experimental results prove the full capability of our system to shape the acoustic periodic wave-packet sequences by tuning q at a fixed delay ΔT that ranges up to $0.5T$. Moreover, the improved modelling by introducing nonlinear corrections and a heuristic-analytical method, matches

Optics EXPRESS

very well with the experiment in the q range from 3/27 to 67/27 and in all considered ΔT up to $0.5T$. The proposed modelling enables us to reasonably explain all the intriguing experimental features including the restriction range, the minimum point determination rule, and the comb component selection rule in acoustic amplitude and phase variations.

Theoretically, the demonstration of acoustic manipulations in the ΔT-q space by simultaneous adjustment of the second pump delay ΔT and the pump intensity ratio q, can be directly available based on our modelling, indicating that it is possible to synthesize a variety of acoustic wave-packet sequences with desired characteristics by tuning q and ΔT.

5. Conclusion

Acoustic manipulation via coherent optical control in a MQW structure is demonstrated by a double-pump-pulse configuration in an Yb:KYW based ASOPS system operating at 1 GHz. By tuning the delay of the second pump pulse with respect to the first pump pulse and the pump intensity ratio, it is possible to modulate the amplitude and the phase of comb-like coherent acoustic phonons excited in a MQW - saturable absorber of a SESAM structure. Abundant experimental results prove that the periodic acoustic wave-packet sequence can be flexibly shaped in terms of wave-packet amplitudes, wave-packet profiles, wave-packet periods, wave-packet widths, and single-period oscillation phase shifts, which refers to a quasi-arbitrary acoustic waveform synthesis by combining various amplitude and phase modulations. The acoustic manipulation by fine tuning the second pump delay within the half wave-packet period is investigated, which reveals a periodic variation of both the spectral amplitude and phase. Meanwhile, the acoustic modulation by fine tuning the pump intensity ratio results in spectral amplitude variations with a zero valley and spectral phase variations with a phase leap only at certain second pump pulse delays when the pump intensity ratio is around 1:1. Moreover, we can proceed from a very low pump power for acoustic manipulations, which benefits from the high detection sensitivity in our Yb:KYW lasers based high-speed ASOPS system. The experimental acoustic manipulation can be well explained in a wide range by a simplified model, enabling us to understand critical spectral features such as the periodicity, the minimum points of amplitude, the selection rule of suppressed comb components, and the upper boundary of the phase and amplitude, and to predict the acoustic phonon shaping where the experiments are absent. More optical parameters in our system could be potentially tuned such as the pump wavelengths, the pump polarization and the pump pulse shape, in order to further enhance the already achieved level of control.

The possibility to optically tailor acoustic wave-packets and acoustic combs in the GHz range by ultrafast lasers is a prerequisite for advanced laser-enabled coherent phonon applications (e.g. acoustic pulse shapers, acoustic field filters, tunable saser). The result of our acoustic manipulation also implies that, acoustic frequencies can be obtained via the spectral amplitude or phase variation period by tuning the second pump delay, and that the unwanted acoustics induced by back-side pump light reflections can be eliminated via destructive interferences by sending the second pump pulse to the sample at a proper time delay and pump intensity. From a general point of view, our research results demonstrate that the progress in ultrafast optics keeps driving the progress in its applications such as picosecond laser ultrasonics including spectroscopy based on the laser-monitored coherent acoustic phonons.

Funding

Deutsche Forschungsgemeinschaft (DFG) through SFB 767, Chinese Scholarship Council (CSC).

Optics EXPRESS

Acknowledgments

Changxiu Li acknowledges Nico Krauß and Gerhard Schäfer for their great experimental support at the early stage, and thanks Lukas Ebner and Oliver Kliebisch for their helpful discussions in the early single-pump-pulse experiment.

References

1. T. Dekorsy, G. C. Cho, and H. Kurz, *Light scattering in solids VIII* (Springer-Verlag, 2000), Chap. 4.
2. V. E. Gusev and A. A. Karabutov, *Laser Optoacoustics* (AIP, 1993).
3. Y.-C. Wen, L.-C. Chou, H.-H. Lin, V. Gusev, K.-H. Lin, and C.-K. Sun, "Efficient generation of coherent acoustic phonons in (111) InGaAs/GaAs multiple quantum wells through piezoelectric effects," Appl. Phys. Lett. **90**(17), 172102 (2007).
4. R. Merlin, "Generating coherent THz phonons with light pulses," Solid State Commun. **102**(2–3), 207–220 (1997).
5. M. Grossmann, M. Klingele, P. Scheel, O. Ristow, M. Hettich, C. He, R. Waitz, M. Schubert, A. Bruchhausen, V. Gusev, E. Scheer, and T. Dekorsy, "Femtosecond spectroscopy of acoustic frequency combs in the 100-GHz frequency range in Al/Si membranes," Phys. Rev. B Condens. Matter Mater. Phys. **88**(20), 205202 (2013).
6. K. Hitachi, M. Someya, A. Ishizawa, T. Nishikawa, and H. Gotoh, "Characterization of longitudinal acoustic phonons in InGaAsP multiple quantum wells by asynchronous optical sampling," Appl. Phys. Lett. **113**(20), 201102 (2018).
7. D. Mounier, P. Picart, P. Babilotte, P. Ruello, J.-M. Breteau, T. Pézeril, G. Vaudel, M. Kouyaté, and V. Gusev, "Jones matrix formalism for the theory of picosecond shear acoustic pulse detection," Opt. Express **18**(7), 6767–6778 (2010).
8. G. Garrett, J. Whitaker, A. Sood, and R. Merlin, "Ultrafast optical excitation of a combined coherent-squeezed phonon field in $SrTiO_3$," Opt. Express **1**(12), 385–389 (1997).
9. J. D. G. Greener, A. V. Akimov, V. E. Gusev, Z. R. Kudrynskyi, P. H. Beton, Z. D. Kovalyuk, T. Taniguchi, K. Watanabe, A. J. Kent, and A. Patanè, "Coherent acoustic phonons in van der Waals nanolayers and heterostructures," Phys. Rev. B **98**(7), 075408 (2018).
10. R. Venkatasubramanian, E. Siivola, T. Colpitts, and B. O'Quinn, "Thin-film thermoelectric devices with high room-temperature figures of merit," Nature **413**(6856), 597–602 (2001).
11. W. Zhu, C. Wang, M. Sun, S. Li, J. Zhai, and T. Lai, "Characterization of Femtosecond laser-irradiation crystallization and structure of multiple periodic $Si/Sb_{80}Te_{20}$ nanocomposite films by coherent phonon spectroscopy," Opt. Express **19**(23), 22684–22691 (2011).
12. K. Makino, J. Tominaga, and M. Hase, "Ultrafast optical manipulation of atomic arrangements in chalcogenide alloy memory materials," Opt. Express **19**(2), 1260–1270 (2011).
13. L. X. Yang, G. Rohde, T. Rohwer, A. Stange, K. Hanff, C. Sohrt, L. Rettig, R. Cortés, F. Chen, D. L. Feng, T. Wolf, B. Kamble, I. Eremin, T. Popmintchev, M. M. Murnane, H. C. Kapteyn, L. Kipp, J. Fink, M. Bauer, U. Bovensiepen, and K. Rossnagel, "Ultrafast modulation of the chemical potential in $BaFe_2As_2$ by coherent phonons," Phys. Rev. Lett. **112**(20), 207001 (2014).
14. T. F. Nova, A. Cartella, A. Cantaluppi, M. Först, D. Bossini, R. V. Mikhaylovskiy, A. V. Kimel, R. Merlin, and A. Cavalleri, "An effective magnetic field from optically driven phonons," Nat. Phys. **13**(2), 132–136 (2017).
15. A. H. Safavi-Naeini, D. V. Thourhout, R. Baets, and R. V. Laer, "Controlling phonons and photons at the wavelength scale: integrated photonics meets integrated phononics," Optica **6**(2), 213–232 (2019).
16. P. Sesin, P. Soubelet, V. Villafañe, A. E. Bruchhausen, B. Jusserand, A. Lemaître, N. D. Lanzillotti-Kimura, and A. Fainstein, "Dynamical optical tuning of the coherent phonon detection sensitivity in DBR-based GaAs optomechanical resonators," Phys. Rev. B Condens. Matter Mater. Phys. **92**(7), 075307 (2015).
17. N. D. Lanzillotti-Kimura, A. Fainstein, and B. Jusserand, "Towards GHz-THz cavity optomechanics in DBR-based semiconductor resonators," Ultrasonics **56**, 80–89 (2015).
18. M. Cardona and G. Güntherodt, *Light scattering in solids V* (Springer-Verlag, 1989).
19. A. Bartels, T. Dekorsy, H. Kurz, and K. Köhler, "Coherent zone-folded longitudinal acoustic phonons in semiconductor superlattice: excitation and detection," Phys. Rev. Lett. **82**(5), 1044–1047 (1999).
20. K. Ishioka, A. Beyer, W. Stolz, K. Volz, H. Petek, U. Höfer, and C. J. Stanton, "Coherent optical and acoustic phonons generated at lattice-matched GaP/Si(0 0 1) heterointerfaces," J. Phys. Condens. Matter **31**(9), 094003 (2019).
21. J. S. Yahng, Y. D. Jho, K. J. Yee, E. Oh, J. C. Woo, D. S. Kim, G. D. Sanders, and C. J. Stanton, "Probing strained InGaN/GaN nanostructures with ultrashort acoustic phonon wave packets generated by femtosecond lasers," Appl. Phys. Lett. **80**(25), 4723–4725 (2002).
22. K. Seeger, *Semiconductor physics*, (Springer, 2004), Chapter 11.
23. C. S. Kim, J. H. Kim, H. Jeong, Y. D. Jho, H. K. Kwon, H. S. Lee, J. S. Park, K. Song, S. H. Kim, Y. J. Kim, D. Lee, and K. J. Yee, "Control of coherent acoustic phonon generation with external bias in InGaN/GaN multiple quantum wells," Appl. Phys. Lett. **100**(10), 101105 (2012).
24. A. Bruchhausen, J. Lloyd-Hughes, M. Hettich, R. Gebs, M. Grossmann, O. Ristow, A. Bartels, M. Fischer, M. Beck, G. Scalari, J. Faist, A. Rudra, P. Gallo, E. Kapon, and T. Dekorsy, "Investigation of coherent acoustic

Optics EXPRESS

phonons in terahertz quantum cascade laser structures using femtosecond pump-probe spectroscopy," J. Appl. Phys. **112**(3), 033517 (2012).
25. O. Matsuda, T. Tachizaki, T. Fukui, J. J. Baumberg, and O. B. Wright, "Acoustic phonon generation and detection in GaAs/$Al_{0.3}Ga_{0.7}As$ quantum wells with picosecond laser pulses," Phys. Rev. B Condens. Matter Mater. Phys. **71**(11), 115330 (2005).
26. W.-R. Liu, J.-H. Lin, J.-S. Chen, H.-M. Cheng, S.-J. Li, H.-R. Chen, C.-H. Hsu, and W.-F. Hsieh, "Saturation and beating of acoustic phonon oscillations excited near the exciton resonance of strained polar ZnO/$Zn_{0.8}Mg_{0.2}O$ multiple quantum wells," RSC Advances **8**(15), 7980–7987 (2018).
27. A. Bartels, T. Dekorsy, H. Kurz, and K. Köhler, "Coherent control of acoustic phonons in semiconductor superlattices," Appl. Phys. Lett. **72**(22), 2844–2846 (1998).
28. D. C. Heinecke, O. Kliebisch, J. Flock, A. Bruchhausen, K. Köhler, and T. Dekorsy, "Selective excitation of zone-folded phonon modes within one triplet in a semiconductor superlattice," Phys. Rev. B Condens. Matter Mater. Phys. **87**(7), 075307 (2013).
29. U. Ozgür, C.-W. Lee, and H. O. Everitt, "Control of coherent acoustic phonons in semiconductor quantum wells," Phys. Rev. Lett. **86**(24), 5604–5607 (2001).
30. G.-W. Chern, K.-H. Lin, Y.-K. Huang, and C.-K. Sun, "Spectral analysis of high-harmonic coherent acoustic phonons in piezoelectric semiconductor multiple quantum wells," Phys. Rev. B Condens. Matter Mater. Phys. **67**(12), 121303 (2003).
31. S.-J. Yu and M. Ouyang, "Coherent discriminatory modal manipulation of acoustic phonons at the nanoscale," Nano Lett. **18**(2), 1124–1129 (2018).
32. K. O'Brien, N. D. Lanzillotti-Kimura, J. Rho, H. Suchowski, X. Yin, and X. Zhang, "Ultrafast acousto-plasmonic control and sensing in compex nanostructures," Nat. Commun. **5**, 5042 (2014).
33. D. H. Hurley, R. Lewis, O. B. Wright, and O. Matsuda, "Coherent control of gigahertz surface acoustic and bulk phonons using ultrafast optical pulses," Appl. Phys. Lett. **93**(11), 113101 (2008).
34. C.-T. Yu, K.-H. Lin, C.-L. Hsieh, C.-C. Pan, J.-I. Chyi, and C.-K. Sun, "Generation of frequency-tunable nanoacoustic waves by optical coherent control," Appl. Phys. Lett. **87**(9), 093114 (2005).
35. X. Shen, Z. Lu, Y. P. Timalsina, T.-M. Lu, M. Washington, and M. Yamaguchi, "Coherent phonon transport measurement and controlled acoustic excitations using tunable acoustic phonon source in GHz-sub THz Range with variable bandwidth," Sci. Rep. **8**(1), 7054 (2018).
36. C.-K. Sun, Y.-K. Huang, J.-C. Liang, A. Abare, and S. P. Denbaars, "Coherent optical control of acoustic phonon oscillations in InGaN/GaN multiple quantum wells," Appl. Phys. Lett. **78**(9), 1201–1203 (2001).
37. A. M. Weiner, "Ultrafast optical pulse shaping: a tutorial review," Opt. Commun. **284**(15), 3669–3692 (2011).
38. A. Bartels, R. Cerna, C. Kistner, A. Thoma, F. Hudert, C. Janke, and T. Dekorsy, "Ultrafast time-domain spectroscopy based on high-speed asynchronous optical sampling," Rev. Sci. Instrum. **78**(3), 035107 (2007).
39. C. Li, N. Krauß, G. Schäfer, L. Ebner, O. Kliebisch, J. Schmidt, S. Winnerl, M. Hettich, and T. Dekorsy, "High-speed asynchronous optical sampling based on GHz Yb:KYW oscillators," Opt. Express **25**(8), 9204–9212 (2017).
40. C. Li, V. Gusev, E. Dimakis, T. Dekorsy, and M. Hettich, "Broadband photo-excited coherent acoustic frequency combs and mini-Brillouin-zone modes in a MQW-SESAM structure," Appl. Sci. (Basel) **9**(2), 289 (2019).
41. M. E. Levinshtein and M. Shur, "Gallium Arsenide (GaAs)," in *Handbook Series on Semiconductor Parameters: Vol. 1*, M. E. Levinshtein, S. L. Rumyantsev, and M. Shur, eds. (World Scientific, 1996).
42. P. Ruello and V. E. Gusev, "Physical mechanisms of coherent acoustic phonons generation by ultrafast laser action," Ultrasonics **56**, 21–35 (2015).
43. U. Keller, "Recent developments in compact ultrafast lasers," Nature **424**(6950), 831–838 (2003).
44. D. J. H. C. Maas, B. Rudin, A.-R. Bellancourt, D. Iwaniuk, S. V. Marchese, T. Südmeyer, and U. Keller, "High precision optical characterization of semiconductor saturable absorber mirrors," Opt. Express **16**(10), 7571–7579 (2008).
45. M. Rüfenacht, S. Tsujino, Y. Ohno, and H. Sakaki, "Delayed luminescence induced by intersubband optical excitation in a charge transfer double quantum well structure," Appl. Phys. Lett. **70**(9), 1128–1130 (1997).

129.247.247.239 {ts '2019-07-24 06:38:21'}